Master's thesis

Front motion in Allen-Cahn-type equations

submitted by Fenna Stegemerten

First examiner: Prof. Dr. Uwe Thiele
Second examiner: Priv. Doz. Dr. Svetlana Gurevich

Institut für Theoretische Physik
Westfälische-Wilhelms-Universität Münster

January 24, 2018

Contents

Introduction

The Allen-Cahn equation is a popular model equation in nonlinear physics. It describes possible phase transition dynamics in multistable systems close to phase transitions of non-conserved order parameter fields. For example, the behavior of the magnetization density $m(x,t)$ in a ferromagnet can be described by a coarse-grained free energy density that is identical to the free energy density of the Allen-Cahn equation. Moreover, the time evolution of m can indeed be modeled by the Allen-Cahn equation [1]. It is possible, that the system corresponds to an arrangement of local equilibrium states. The interfaces between these states we call front. They might rest or move. Throughout this thesis we examine the behavior of the order parameter $\phi(x,t)$ when changing an external field or the chemical potential μ within the Allen-Cahn equation. Changing μ from zero allows fronts to move and we are interested in the velocity of such fronts. Among others, we are also interested in propagation into unstable states. Such fronts occur when systems are suddenly quenched into the unstable state and small perturbations are able to grow and develop certain patterns which spread out over the whole domain. This can for example be found in Taylor-Couette Flow [2]. When the angular velocity of the inner cylinder is low the Couette flow is stable. However, if the velocity is suddenly increased, the Couette flow becomes linearly unstable (but the system is still in this state as the velocity has been changed rapidly) and the Taylor-vortex flow propagates inwards from the ends of the cylinder. Another front appears in Rayleigh-Bénard systems when the heat flux is suddenly increased. The convective vortex fronts propagate into the unstable conductive state [3]. Moreover, front propagation into unstable states is studied in crystal growth [4] and in the context of chemical reactions [5]. This thesis deals with Allen-Cahn-type equations. Therefore, we introduce the simple cubic Allen-Cahn equation in section 1. Even though the cubic Allen-Cahn equation is often studied [1], we give a complete overview of all possible fronts occurring in the system as well as introduce the analytical and numerical analysis of these fronts. In the first section we also introduce the linear marginal stability analysis and contrast it to the nonlinear marginal stability analysis. This allows us to determine different front types and the corresponding velocities. In the second section we consider a quintic Allen-Cahn equation such equations already attracted interest as e.g. in [6, 7, 8, 9]. However, the equations under examination in the referred literature allow analytical solutions because the derivative of the local energy density can be brought into product form. Thus, one is able to find the homogenous solutions of the system. The quintic Allen-Cahn equation we study is analytically impossible to solve and we therefore analyze the occurring front profiles numerically towards the criterions introduced in the first

section. The third section concerns a non-variational cubic Allen-Cahn equation. Non-variational means that the time evolution of the order parameter is not driven by the minimization of the free energy functional. The non-variational term we add here has also been studied for the Swift-Hohenberg equation [10]. The equation we study in this section describes front propagation in a liquid crystal light valve [11]. We present analytically the shift in velocity for the transition from a variational front to a non-variational front at $\mu = 0$ and compare this to our numerical results. Furthermore, we present the numerically determined bifurcation diagrams for a variational as well as a non-variational system. Finally, we will give a conclusion and an outlook.

1. Fronts in the cubic Allen-Cahn equation

1.1. The cubic Allen-Cahn equation

As this thesis deals with Allen-Cahn-type equations, we firstly introduce the simple cubic Allen-Cahn equation similarly to [1] and [12]. The time evolution of the order parameter field $\phi(x,t)$ is driven by the thermodynamic force, which is a functional derivative of the free energy $\mathcal{F}$:

$$\frac{\partial \phi}{\partial t} = -\frac{\delta \mathcal{F}}{\delta \phi} \tag{1.1}$$

$$\mathcal{F} = \int \mathrm{d}x \left[\frac{1}{2} \left(\frac{\partial}{\partial x} \phi \right)^2 + f(\phi) \right] . \tag{1.2}$$

The system always tries to reach thermodynamic equilibrium which means to minimize the free energy. Here, the first term in the integral of the free energy is a distortion term, taking into account the gradient of the order parameter field which corresponds to the interface energy [1]. The second term is the local energy density $f(\phi)$, that here has a double well structure

$$f(\phi) = -\frac{1}{2}\phi^2 + \frac{1}{4}\phi^4 - \mu\phi \,, \tag{1.3}$$

where μ is the chemical potential. Figure 1.1 shows $-f(\phi)$. As we are studying Allen-Cahn like equations in this thesis, we will examine other local energy densities in further sections. Inserting (1.3) and (1.2) into (1.1) yields the cubic Allen-Cahn equation

$$\frac{\partial \phi}{\partial t} = \frac{\partial^2 \phi}{\partial x^2} - f'(\phi) = \frac{\partial^2 \phi}{\partial x^2} + \phi - \phi^3 + \mu \,. \tag{1.4}$$

Here the prime denotes derivative with respect to ϕ. The homogenous steady state solutions need to satisfy

$$-f'(\phi) = \phi - \phi^3 + \mu = 0 \,. \tag{1.5}$$

This equation can be solved by applying the cardanic formulas, which results for $-\frac{2}{3\sqrt{3}} < \mu < \frac{2}{3\sqrt{3}}$ in

$$\phi^0 = -\sqrt{\frac{4}{3}}\cos\left(\frac{1}{3}\arccos\left(\frac{3\sqrt{3}}{2}\mu\right) + \frac{\pi}{3}\right) \tag{1.6a}$$

$$\phi^+ = \sqrt{\frac{4}{3}}\cos\left(\frac{1}{3}\arccos\left(\frac{3\sqrt{3}}{2}\mu\right)\right) \tag{1.6b}$$

$$\phi^- = -\sqrt{\frac{4}{3}}\cos\left(\frac{1}{3}\arccos\left(\frac{3\sqrt{3}}{2}\mu\right) - \frac{\pi}{3}\right) . \tag{1.6c}$$

ϕ^+ and ϕ^- are stable states, whereas ϕ^0 is an unstable state. By introducing μ we not only present a physically relevant quantity, but also a more general parameter than those found in most used parametrizations [13, 9, 14, 15, 16]. Because the roots in (1.6) depend on μ we can transform $f'(\phi)$ into product form. Thus, every factor of this form depends on μ. Most of the equations considered in the literature study the system's behavior when varying a paramteter in only one factor of the product form. Hence, we introduce a way to change parameters in all factors at the same time. This is of course strongly nonlinear and does not simplify many calculations but it might be easier to realize in experiments, as μ is a physical (and chemical) quantity.

As we are interested in the front propagation into unstable states and its velocity, we transform (1.4) into the comoving frame ($\xi = x - vt$). Thus, fronts move to the right, if $v > 0$ and to the left otherwise. The corresponding ordinary differential equation is:

$$\frac{\mathrm{d}^2\phi}{\mathrm{d}\xi^2} = -v\frac{\mathrm{d}\phi}{\mathrm{d}\xi} - \frac{\mathrm{d}\left(-f(\phi)\right)}{\mathrm{d}\phi} . \tag{1.7}$$

This equation is familiar from classical mechanics as it describes the motion of a particle moving in a potential $V = -f(\phi)$ with friction v, where ξ denotes time (see figure 1.1).

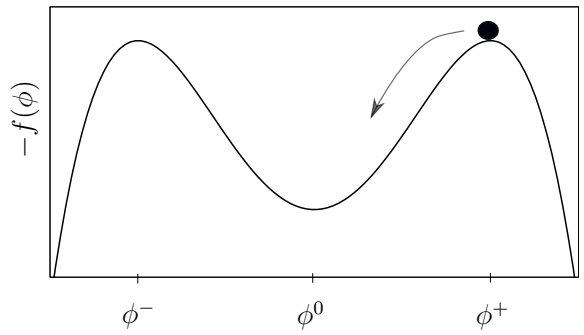

Figure 1.1: The energy density $f(\phi)$ can be described as a potential $V = -f(\phi)$ in the mechanical analogon. Here it is shown for $\mu = 0$.

Regarding the mechanical analogon where v acts as a friction, we find that for $\mu = 0$ and $v \neq 0$ a particle starting at the top of either of the two hills at ϕ^+ or ϕ^-, will always (for any $v > 0$) end up at ϕ^0, the bottom of the valley. However, we find that the front approaches one particular velocity [15]. For example if $\mu = 0$ we find that $v = 2.0$. This friction corresponds to the smallest friction for which the particle moves directly into the state ϕ^0 without overshooting. Thus, there must be a dynamical selection mechanism such that only one particular velocity occurs. In the next section we will explain this selection criterion which is called linear marginal stability criterion.
Multiplying (1.7) by $\frac{\mathrm{d}\phi}{\mathrm{d}\xi}$ and integrating over ξ from $-\infty$ to ∞ yields

$$-v\int_{-\infty}^{\infty}\left(\frac{\mathrm{d}\phi}{\mathrm{d}\xi}\right)^2\mathrm{d}\xi = \frac{1}{2}\int_{-\infty}^{\infty}\frac{\mathrm{d}}{\mathrm{d}\xi}\left(\frac{\mathrm{d}\phi}{\mathrm{d}\xi}\right)^2\mathrm{d}\xi - \int_{-\infty}^{\infty}\left(\frac{\mathrm{d}f}{\mathrm{d}\xi}\right)\mathrm{d}\xi\,. \tag{1.8}$$

The first term on the right-hand side is zero, due to the Neumann boundary conditions. We require:

$$\phi = \phi^f \qquad \text{for} \quad \xi \to -\infty \tag{1.9a}$$
$$\phi = \phi^i \qquad \text{for} \quad \xi \to \infty\,, \tag{1.9b}$$

where ϕ^i denotes the initial state and ϕ^f denotes the final state. Note, that throughout this thesis we always consider a propagation to the right, when $v > 0$, thus the initial state is the one, the front propagates into. This is sketched in figure 1.2.

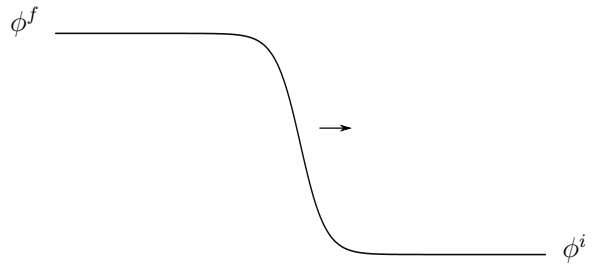

Figure 1.2: When $v > 0$ the front moves to the right. Thus, the final state ϕ^f invades the initial state ϕ^i.

However, we will also come across front solutions with $v < 0$, where the front moves to the left. Then

$$\phi = \phi^f \qquad \text{for} \quad \xi \to \infty \tag{1.10a}$$

$$\phi = \phi^i \qquad \text{for} \quad \xi \to -\infty\,. \tag{1.10b}$$

Thus, we can simplify (1.8) (considering the different limits of integration) to

$$v = \pm \frac{f\left(\phi^i\right) - f\left(\phi^f\right)}{\int_{-\infty}^{\infty} \left(\frac{\mathrm{d}\phi}{\mathrm{d}\xi}\right)^2 \mathrm{d}\xi}\,, \tag{1.11}$$

where the positive sign denotes motion to the right and the negative sign motion to the left, respectively.
So, the velocity depends on the difference between energy densities or, in the mechanical analogon on the difference in potential values. However, this is only satisfied, if the differential equation 1.7 is variational. For non-variational equations we discuss the velocity dependence in section 3.

1.2. Linear marginal stability analysis

In this section we will focus on the linear marginal stability analysis and therefore, develop the criterion for linear marginal stability analogously to [17].
As discussed in the previous section, there is a dynamical selection problem for propagation into unstable states. The selected velocity is called the linear marginal velocity. In order to understand the concept of the linear marginal stability analysis we firstly approach the idea in a more intuitive way followed by a mathematical explanation.
To start with, we imagine crystal growth as illustrated in figure 1.3. The crystal consists of two different facets A and B. Facets A move slower than facets B $v_A < v_B$. However, as the crystal grows, facets A are dominating the structure of

the crystal until finally facets B are vanish completely. Moreover, we can say that the crystal will eventually grow with the slowest velocity v_A.

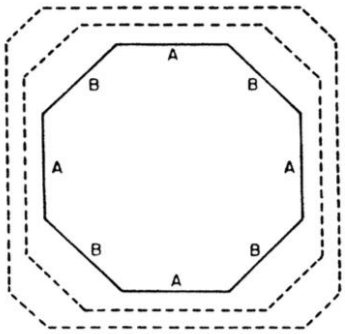

Figure 1.3: Crystal growth: The facets A move slower than facets B. Hence, the long time behavior is dominated by the velocity of facets A. Finally, facets B vanish completely.[1]

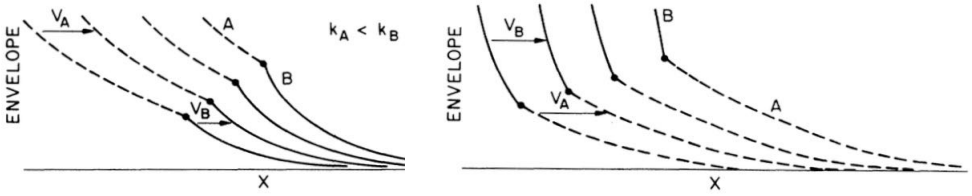

Figure 1.4: Front profiles with two different parts in steepness and velocity. If the steeper and slower part is to the right of the shallower and faster part, the long time behavior is dominated by the slowest velocity (left). This is not valid, if the order is changed (right). Hence, we require sufficiently steep initial conditions.[2]

This mechanism can also be found in front motion. The front profiles depicted in figure 1.4 are opposed to reality not continuous. However, in order to understand the mechanism this presentation is more convenient. Besides, we argue similarly for continuous front profiles. There are two different parts within the profile on the left in figure 1.4. For the two parts ϕ_A and ϕ_B within the front profile we use the ansatz

$$\phi_i \sim \mathrm{e}^{k_i x} \qquad \text{with} \quad i = A, B\,, \tag{1.12}$$

where k is called the wave vector [3]. Part A with wave vector k_A and velocity v_A is less steep than part B with velocity v_B and wave vector k_B, as $k_A < k_B$. Furthermore, $v_B < v_A$ and we find that part B dominates the long time behavior

[1] Figure is taken from [17]
[2] Figure is taken from [17]
[3] We name $k \in \mathbb{C}$ wave vector although in the classical sense only the imaginary part $\mathrm{Im}(k)$ is called the wave vector

as the crossing point of the two parts moves up in space until part A eventually vanishes. So again, we find that the whole front will approach the velocity of its slowest part. However, as shown in figure 1.4 on the right, this strongly depends on the order of the parts within the profile. Thus, if the steeper part is to the left of the shallower part, the long time behavior is dominated by part A. So, sufficiently steep initial conditions need to be satisfied. A more detailed description about what 'sufficiently steep' means is given in [14]. Here, we only refer to the result of their studies, that the profile needs to fall off at least with the linear marginal wave vector k_l. So sufficiently steep implies that any initial profile with wave vector k needs to satisfy $k > k_l$.

Next, we will study the linear marginal stability analysis in a more mathematical way following [17]. Firstly, we determine the stability of a front solution. Thus, we obtain a necessary condition for stability which leads us to the marginal stability point. Secondly, we are going to analyze the front's approach to this constant velocity.
The general type of partial differential equation that we examine is

$$\frac{\partial \phi}{\partial t} = \frac{\partial^2 \phi}{\partial x^2} - f'(\phi)\,. \tag{1.13}$$

Considering propagation into the unstable state ϕ^0, we first linearise (1.13) about ϕ^0 by inserting $\phi = \phi^0 + \epsilon\tilde{\phi}$ and neglect order ϵ^2 and higher. Thus, we only focus on the leading edge of the front and assume that the behavior of the whole front is subject to the behavior of the leading edge. This is why the method is called *linear* stability analysis. The linearization yields

$$\tilde{\phi}_t = g(\tilde{\phi}, \tilde{\phi}_{xx}) = \tilde{\phi}_{xx} - f''(\phi^0)\tilde{\phi}\,, \tag{1.14}$$

where g is a linear function in $\tilde{\phi}$ and $\tilde{\phi}_{xx}$ and the subscripts x and t denote derivatives with respect to x and t, respectively. Note, that f can also depend on derivatives of ϕ with respect to x: $f = f(\phi, \phi_x, \phi_{xx})$. However, the argument is similar to the one given here and can e.g. be found in [17]. For reasons of simplification we restrict our argument to local energy densities $f = f(\phi)$.
We now introduce the ansatz

$$\tilde{\phi} = e^{-u}\,, \tag{1.15}$$

and insert this into (1.14), which leads us to a differential equation for the behavior of the exponent u, which includes all relevant information for the behavior of the leading edge

$$u_t = -G(u_x, u_{xx}) = -u_x^2 + u_{xx} + f''(\phi^0)\,. \tag{1.16}$$

Due to the product rule, G is a nonlinear function in general. To find the front's velocity and to understand how the velocity v depends on the wave vector (steepness of the leading edge) k, we transform to the frame moving with velocity v with $\xi = x - vt$. Hence, the derivatives change likewise

$$(x,t) \to (\xi(x,t),t) \tag{1.17a}$$

$$\left.\frac{\partial}{\partial x}\right|_t \to \xi_x \left.\frac{\partial}{\partial \xi}\right|_t = \left.\frac{\partial}{\partial \xi}\right|_t \tag{1.17b}$$

$$\left.\frac{\partial}{\partial t}\right|_x \to \left.\frac{\partial}{\partial t}\right|_\xi + \xi_t \left.\frac{\partial}{\partial \xi}\right|_t = \left.\frac{\partial}{\partial t}\right|_\xi - v \left.\frac{\partial}{\partial \xi}\right|_t . \tag{1.17c}$$

The $|_t$ indicate which variable is held constant for the derivative in order to understand the transformation. Thus, (1.16) transforms to:

$$u_t = v u_\xi - G(u_\xi, u_{\xi\xi}) , \tag{1.18}$$

where $u_t = \left.\frac{\partial}{\partial t}\right|_\xi u(\xi,t)$ and $G(u_\xi, u_{\xi\xi}) = G(u_x, u_{xx})$ because $\frac{\partial \xi}{\partial x} = 1$. Moreover, we claim that in the laboratory frame

$$u = -\omega(k)t + kx , \tag{1.19}$$

where k is the wave vector and ω the frequency, both can be complex. Employing $x = \xi + vt$ (1.19) transforms to

$$u = -\omega(k)t + kvt + k\xi , \tag{1.20}$$

Throughout this thesis, we require k to be independent of ξ. Therefore, $u_\xi = k$ and $u_{\xi\xi} = 0$. Furthermore, inserting (1.20) into (1.18) yields

$$kv - \omega(k) = kv - G(k,0) \tag{1.21}$$

$$\Rightarrow G(k,0) = \omega(k) = g(1,k^2) , \tag{1.22}$$

as g is a linear function. Because we require the steady state solutions in the comoving frame to move with constant velocity, we claim that $\mathrm{Re}\,(u_t) = 0$ in (1.18). Thus, in the comoving frame the envelope rests but oscillations may occur. The requirement applied to (1.18) using (1.22) yields

$$\mathrm{Re}(vk - G(k,0)) = 0 \tag{1.23}$$

$$v(k) = \frac{\omega^r(k)}{k^r} , \tag{1.24}$$

where the superscript r denotes the real part. This is the envelope velocity of the front. In order to find the velocity, the front profile eventually approaches, we need to study the front stability. Analyzing the stability of steady state solutions in the comoving frame, we consider a small perturbation ϵ of u. By linearizing (1.18) we obtain

$$u_t + \epsilon_t = vu_\xi - G(u_\xi, u_{\xi\xi}) + v\epsilon_\xi - G_{u_\xi}(u_\xi, u_{\xi\xi})\epsilon_\xi - G_{u_{\xi\xi}}(u_\xi, u_{\xi\xi})\epsilon_{\xi\xi} \tag{1.25a}$$

$$\Leftrightarrow \epsilon_t = v\epsilon_\xi - G_{u_\xi}(u_\xi, u_{\xi\xi})\epsilon_\xi - G_{u_{\xi\xi}}(u_\xi, u_{\xi\xi})\epsilon_{\xi\xi}\,. \tag{1.25b}$$

Here G_{u_ξ} and $G_{u_{\xi\xi}}$ are the derivatives of G with respect to u_ξ and $u_{\xi\xi}$, respectively. We neglected higher order in ϵ. Note that (with (1.22))

$$G_{u_\xi}(u_\xi, u_{\xi\xi}) = \omega'(k)\,, \tag{1.26}$$

where the prime denotes derivative with respect to k.
The stability criterion requires bounded perturbations to decay. Besides, we consider G to only depend on u_ξ, because of (1.22). Thus, for $\epsilon \sim \mathrm{e}^{-\alpha\xi}$ and $|\alpha|$ small (because we study small perturbations), (1.25b) becomes:

$$\epsilon_t = -\left(v - \omega'(k)\right)\alpha\epsilon\,. \tag{1.27}$$

In order not to increase over time, perturbations need to fulfill:

$$\mathrm{Re}\left(\frac{\epsilon_t}{\epsilon}\right) \leq 0 \tag{1.28a}$$

$$\Leftrightarrow \mathrm{Re}\left(-\left(v - \omega'(k)\right)\alpha\right) \leq 0\,. \tag{1.28b}$$

We focus on small perturbations with $\mathrm{Re}(\alpha) > 0$ (in order for perturbations to decay in space), thus we require:

$$\mathrm{Im}\left(\omega'(k)\right) = 0 \tag{1.29}$$

$$\mathrm{Re}(\omega'(k)) \leq v\,. \tag{1.30}$$

Note that (1.29) must be satisfied as (1.28b) is valid for any small $\alpha \in \mathbb{C}$. Interpreting $\mathrm{Re}(\omega'(k))$ as the group velocity of small perturbations, the stability condition says that the envelope velocity needs to be greater than the group velocity of small perturbations. Otherwise, perturbations would run ahead and the front solution would get unstable. This argument also explains the equality in (1.28a), as the perturbations can not run ahead if the envelope velocity just equals the perturbation's group velocity.
We can express the imaginary part of the wave vector k^i via k^r using condition

(1.29) and accordingly determine $v = v\,(k^r)$.
Since we examine propagation into unstable states, ω^r needs to be finite and positive for $k^r \to 0$, otherwise small perturbations would not grow out of the unstable state. Thus, v in (1.24) diverges for $k^r \to 0$ as ω^r behaves nicely in this limit, and we assume v to have a minimum. In order to determine the extrema we calculate the derivative of $v\,(k^r)$

$$\begin{aligned}\frac{\mathrm{d}v}{\mathrm{d}k^r} &= \frac{\mathrm{d}}{\mathrm{d}k^r}\left(\frac{\omega^r(k)}{k^r}\right)\\ &= \frac{1}{k^r}\left(\frac{\mathrm{d}\omega^r(k)}{\mathrm{d}k^r} - \frac{\omega^r(k)}{k^r}\right)\\ &= \frac{1}{k^r}\left(\mathrm{Re}\left(\frac{\mathrm{d}\omega(k)}{\mathrm{d}k}\right) - v(k)\right) \stackrel{!}{=} 0\,. \end{aligned} \tag{1.31}$$

Comparing the expression in brackets with the stability criterion (1.30) we find that $v\,(k^r)$ has an extremum at the point where stability just changes. Thus, the front is marginal stable and hence, this point is called the linear marginal stability point which satisfies

$$v_l(k) = \mathrm{Re}\left(\frac{\mathrm{d}\omega(k)}{\mathrm{d}k}\right) = \frac{\omega^r(k)}{k^r} \tag{1.32a}$$

$$\mathrm{Im}\left(\frac{\mathrm{d}\omega(k)}{\mathrm{d}k}\right) = 0\,, \tag{1.32b}$$

with v_l being the linear marginal velocity. If the front moves with this linear marginal velocity no perturbations are able to outrun the front profile as their group velocity is just equal to the envelope velocity of the profile.

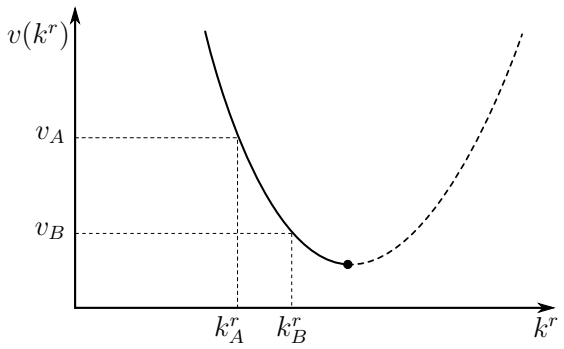

Figure 1.5: The velocity v depending on wave vector k^r. As the asymptotic behavior is dominated by the smallest wave vector we neglect solutions on the dashed line, but focus on the solid line. Thus, fronts with slower velocity are steeper than those with higher velocity.

As (1.18) is a quadratic equation in k (using (1.22)) we obtain two branches for $v\left(k^r\right)$ as depicted in figure 1.5. Because only profiles with smaller wave vector will dominate the asymptotic behavior $x \to \infty$, it suffices to focus on the solid branch.

Not to cause any confusion, we remark, that front profiles moving with velocity $v > v_l$ corresponding to solutions on the black solid branch in figure 1.5, are stable in the sense that perturbations do not change the fact, that the front propagates from a stable state into an unstable state. However, these fronts change their shape (the k-vector changes) and their velocity, until they approach in the long-time behavior the linear marginal velocity.

So far, we found the linear marginal stability point but we also need to show, that a profile with sufficiently steep initial conditions approaches this linear marginal velocity. Therefore, we go back to the laboratory frame and examine if u_x approaches k_l, the wave vector at the marginal stability point. For simplification we introduce

$$q = u_x \,, \tag{1.33}$$

and transform the variables x and t to variables u^r and t because the envelope profile moves with u^r (remember that $u_t^r = 0$ in the comoving frame). Transforming onto these variables implies transforming the derivatives likewise, which yields

$$(x,t) \to (u^r(x,t),t) \tag{1.34a}$$

$$\left.\frac{\partial}{\partial x}\right|_t \to u_x^r \left.\frac{\partial}{\partial u^r}\right|_t = q^r \left.\frac{\partial}{\partial u^r}\right|_t \tag{1.34b}$$

$$\left.\frac{\partial}{\partial t}\right|_x \to \left.\frac{\partial}{\partial t}\right|_u + u_t \left.\frac{\partial}{\partial u^r}\right|_t = \left.\frac{\partial}{\partial t}\right|_u - G^r(q,q_x) \left.\frac{\partial}{\partial u^r}\right|_t \,, \tag{1.34c}$$

where we used (1.16) on the right-hand side in (1.34c). Moreover, we find that

$$\frac{1}{q^r}\frac{\partial^2 u(x,t)}{\partial x \partial t} = \frac{\partial}{\partial u^r}\frac{\partial u(x,t)}{\partial t} = \frac{1}{q^r}\left.\frac{\partial q}{\partial t}\right|_x = \frac{1}{q^r}\left(\left.\frac{\partial q}{\partial t}\right|_u - G^r q_u\right) \,, \tag{1.35}$$

where the subscript u denotes derivative with respect to u^r. In order to analyze the time evolution of q we differentiate (1.16) with respect to u^r and transform

the resulting equation onto our new variables using (1.35)

$$\begin{aligned} \frac{\partial}{\partial u^r} u_t &= -\frac{\partial}{\partial u^r} G(q, q_x) \\ \frac{1}{q^r}\left(\frac{\partial q}{\partial t} - G^r q_u\right) &= -G_q q_u - G_{q_u} q_{uu} \Rightarrow q_t = \left(\frac{G^r}{q^r} - G_q\right) q^r q_u - q^r G_{q_u} q_{uu}\,, \end{aligned} \tag{1.36}$$

where we employed

$$\frac{\partial G}{\partial q_x}\frac{\partial q_x}{\partial u^r} = \frac{\partial G}{\partial q_u} q_{uu}\,. \tag{1.37}$$

We now need to show, that the marginal stability point is an attractive fixed point for (1.36) as $q_t = 0$ implies that the front's shape is constant and following our previous arguments so is the front's velocity. Note, that the term in brackets in (1.36) vanishes at the marginal stability point because $q = k_l$, $G^r(k_l, 0) = \omega^r(k_l)$ and $G_q(k_l, 0) = \omega'(k_l)$. Therefore, we study the two terms on the right-hand side in (1.36) separately and show that they correspond to a stable fixed point at $k = k_l$. Considering

$$q_t = \left(G^r - q^r G_q\right) q_u\,, \tag{1.38}$$

we study the stability of the solution $q = k_l$ by expanding q around this point

$$q(u^r, t) = k_l + \rho(u^r, t) \tag{1.39}$$

and inserting this expansion into the differential equation (1.38) where we only take into account terms up to second order in ρ. Moreover, we assume G to only depend on q, as $q_x = 0$ for (1.19). Thus, we obtain

$$\begin{aligned} \rho_t &= -\left(G^r(k_l) + G^r_q(k_l)\rho - k_l G_q(k_l) - k_l G_{qq}(k_l)\rho - \rho G_q(k_l)\right)\rho_u + \mathcal{O}(\rho^3) \\ &= -\left(G_{qq}(k_l) k_l\right)\rho\rho_u + \mathcal{O}(\rho^3)\,. \end{aligned} \tag{1.40}$$

Moreover, we know about the term in brackets with (1.22) and (1.32)

$$G_{qq}(k_l)k_l = k_l^2 \frac{\mathrm{d}^2 v}{\mathrm{d}k^2}\bigg|_{k=k_l}\,, \tag{1.41}$$

which is positive as k_l is a minimum of $v(k)$. Thus, if we have sufficiently steep initial conditions with $q > k_l$ for large u^r, then ρ_u is positive and hence ρ decays over time. This means, that q approaches k_l over time which implies that v approaches v_l. On the other hand, if initial conditions are such that $q < k_l$, q approaches a smaller value $k < k_l$. This is explained in more detail in [17], we restrain from further explanation as we assume sufficiently steep initial conditions throughout

this thesis.
Eventually, we need to ensure, that

$$q_t = -q^r G_{q_u}(q, q_u) q_{uu} \tag{1.42}$$

has a stable fixed point. Thus we need to show that small perturbation in q decay in time. This analysis depends on each specific equation and we will consider this in the following sections.

Alternatively, the linear marginal stability criterion can be determined via the so called saddle-point method or method of steepest descent which is e.g. explained in [12] and [9]. Here, the saddle point method determines the maximum contribution of an integral. The integral in this case is an integral over all Fourier-modes. Considering the saddle-point method, then leads to the marginal stability point.
Additionally, in [18] they derive the marginal stability point by introducing a test function and integrating the differential equation. Thus the front's velocity can be determined by solving a variational problem. However, the linear marginal velocity turns out to be a necessary condition for the integrals to exist.

1.3. Basic continuation principle

Before we analyze the linear marginal stability of the Allen-Cahn equation, we would like to introduce the basic principle of continuation. Throughout this thesis we work with the continuation program *auto-07p* in order to find solution branches for different parameter sets. In the following, we shortly outline the basic idea of continuation but will neglect to explain all the features of *auto-07p*.
Imagine the equation

$$G(\mathbf{y}, \lambda) = 0\,, \tag{1.43}$$

where $\mathbf{y}$ denotes a n-dimensional solution vector, λ is a parameter and G is a nonlinear operator. In order to find the solution branch in dependence of λ, we implement the so called predictor-corrector method. The basic idea of this method is illustrated in figure 1.6.

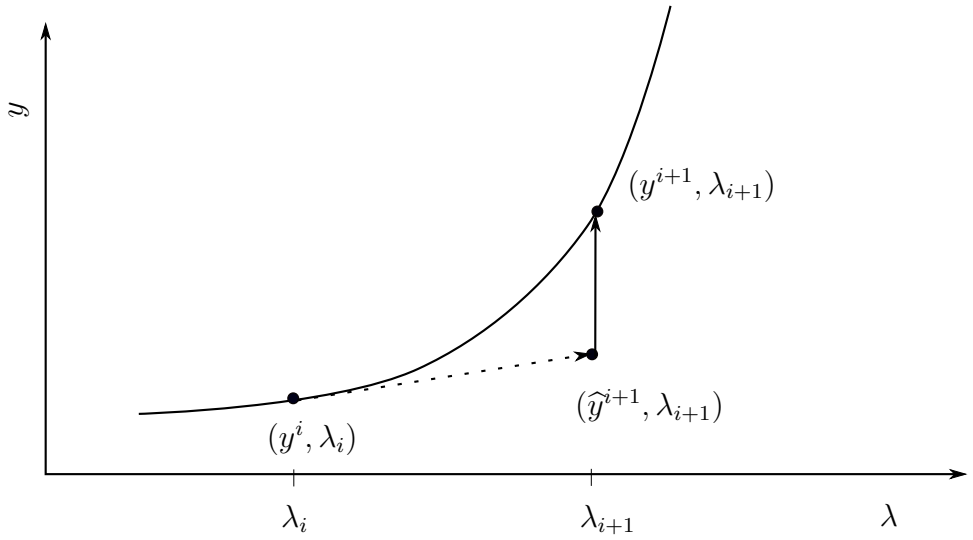

Figure 1.6: Illustration of the predcitor-corrector idea: The dotted arrow follows the tangent direction up to λ_{i+1}. Employting Newton's method yields the correct solution on the $y(\lambda)$- curve. For simplification we only show the one-dimensional case $\mathbf{y} = y$

Starting with a point on the solution branch $(\mathbf{y}^i, \lambda_i)$, we take the tangent of $\mathbf{y}(\lambda)$ in this point as a predictor and then employ Newton's method to obtain the next point on the branch, namely $(\mathbf{y}^{i+1}, \lambda_{i+1})$. Thus. we first need to find the tangent vector. Therefore, we differentiate (1.43) with respect to λ at the i-th solution point and obtain:

$$G_{\mathbf{y}i} \left.\frac{\mathrm{d}\mathbf{y}}{\mathrm{d}\lambda}\right|_{(\mathbf{y}^i, \lambda_i)} + G_{\lambda_i} = 0 \tag{1.44}$$

where $G_{\mathbf{y}}$ is the Jacobian and G_λ is the derivative of G with respect to λ. Hence, solving (1.44) yields the tangent vector $\dfrac{\mathrm{d}\mathbf{y}}{\mathrm{d}\lambda}$ to the i-th solution point. Now, we get the predictor point $(\widehat{\mathbf{y}}^{i+1}, \lambda^{i+1})$ at $\lambda^{i+1} = \lambda^i + \Delta\lambda$ with:

$$\widehat{\mathbf{y}}^{i+1} = \mathbf{y}^i + \Delta\lambda \left.\frac{\mathrm{d}\mathbf{y}}{\mathrm{d}\lambda}\right|_{(\mathbf{y}^i, \lambda_i)} . \tag{1.45}$$

Next, we need to implement Newton's method to find the next solution $\mathbf{y}^{i+1}$ up to a chosen correctness. Note, that this simple continuation fails at saddle-node bifurcations, as there $G_{\mathbf{y}}$ becomes zero. Hence, the arclength s is been introduced as a new parameter and we treat $\lambda(s)$ as the $n+1$-th element of the solution vector. Thus, we need an additional equation in order to solve the problem for the new parameter s. We obtain this additional condition when requiring the local

approximation of the arclength

$$|\Delta \mathbf{y}|^2 + (\Delta\lambda)^2 = (\Delta s)^2 \,. \tag{1.46}$$

For further information regarding continuation we refer to [19, 20].

1.4. Linear marginal stability analysis of the cubic Allen-Cahn equation

Returning to the cubic Allen-Cahn equation i.e.

$$\frac{\partial \phi}{\partial t} = \frac{\partial^2 \phi}{\partial x^2} + \phi - \phi^3 + \mu \,, \tag{1.47}$$

we apply the linear marginal stability analysis. We are interested in the propagation into the unstable state ϕ^0 and only focus on the leading edge of such a front. Therefore, we insert the ansatz $\phi = \phi^0 + \epsilon \mathrm{e}^{-\omega t + kx}$ into (1.47) and only expand to linear order in ϵ:

$$\omega = -k^2 + f''(\phi^0) \,, \tag{1.48}$$

where

$$f(\phi) = -\frac{1}{2}\phi^2 + \frac{1}{4}\phi^4 - \mu\phi \,. \tag{1.49}$$

Employing (1.32) yields the linear marginal stability point

$$\mathrm{Im}\left(\frac{\mathrm{d}\omega(k)}{\mathrm{d}k}\right) = -2k^i = 0 \qquad \Rightarrow k^i = 0 \tag{1.50a}$$

$$-2k^r \stackrel{!}{=} \frac{-\left(k^r\right)^2 + f''(\phi^0)}{k^r} \qquad \Rightarrow k_l = \pm\sqrt{-f''(\phi^0)} \tag{1.50b}$$

$$v_l = \pm 2\sqrt{-f''(\phi^0)} = \pm 2\sqrt{1 - 3\left(\phi^0\right)^2} \,. \tag{1.50c}$$

Inserting (1.6a) into (1.51), we obtain

$$v_l(\mu) = \pm 2\sqrt{1 - 4\left(\cos\left(\frac{1}{3}\arccos\left(\frac{3\sqrt{3}}{2}\mu\right) + \frac{\pi}{3}\right)\right)^2} \,. \tag{1.51}$$

To ensure, that this is indeed an attractive fixed point of (1.36), we need to show, that (1.42) is decaying in time. We first remember that with (1.34b):

$$G_{q_u}(q, q_u)\big|_{q=k_l} = k_l G_{q_x}(q, q_x)\big|_{q=k_l} \,. \tag{1.52}$$

Moreover, linearising (1.47) and inserting the ansatz $\tilde{\phi} \sim \mathrm{e}^{-u}$ we obtain:

$$G(q, q_x) = f''(\phi^0) - q_x + q^2 \,. \tag{1.53}$$

Thus, with (1.52) and (1.53), (1.42) results in:

$$q_t = k_l^2 q_{uu} \,. \tag{1.54}$$

So, perturbations decay and the linear marginal stability point of the cubic Allen-Cahn equation is indeed an attractive fixed point.

One major difference comparing the Allen-Cahn equation (1.47) with the ones employed in the literature [17, 14, 9, 8, 7] is, that we study propagation into an unstable state which depends nonlinearly on the parameter μ whereas in the literature the unstable state is assumed to be constant and usually $\phi^0 = 0$. So, in the following we discuss the behavior of front solutions depending on the parameter μ. But let us first return to the mechanical analogon: By varying μ the potential, in which the particle is moving, is tilted. So, not only the positions of the extrema shift, but also their 'height'. This is why the corresponding friction v needs to be adapted when μ is changed. Otherwise the particle would not end up exactly in either a maximum or a minimum.
With the continuation program *auto-07p* we continue in μ and v.
Remember that we start for the Allen-Cahn equation in *auto-07p* by continuing in the domain-size L.
Therefore, we sinusoidally perturb the unstable state $\phi^0 = 0$ with wavenumber k_c at $\mu = 0$ for domain size $L = \frac{\pi}{k_c}$ and increase the domain size up to $L = 60$ at fixed μ, such that a front between the two stable states develops. During this continuation, v adapts however, stays at $v = 0$ as the front does not move. Starting from the resting front between the two stable states we now continue in μ and let v adapt. As we can not approach infinite domain size we need L to be sufficiently large, but *auto-07p* stops continuation in μ at $L > 60$ for reasons we do not yet understand in detail. We employ Neumann boundary conditions and an integral condition that ensures, the dividing interface to stay at $\xi = 0.5$ in the comoving frame. Hence, we obtain the bifurcation diagram shown in figure 1.7(a).
Even though the Allen-Cahn equation has certain symmetries as $\phi \to -\phi$ when $\mu \to \mu$ and $v \to -v$, we do not restrict the bifurcation diagram to $|\mu|$ and $|v|$. Thus, the behavior especially for more complex systems will become clearer.
The red dashed lines in figure 1.7(a) are the solution branches for fronts between the two maxima ϕ^+ and ϕ^-, as depicted in panel (e). We show in panel (b) the

potential for the critical value $\mu_c = \frac{2}{3\sqrt{3}}$ where the two states ϕ^0 and ϕ^- merge. In the bifurcation diagram (a) we find this point where the red dashed line merges with the blue solid line. Here, the front between the two maxima now develops into a front between the higher maximum (in the mechanical analogon) and the minimum. The example depicted in figure 1.7(c) shows such a front between ϕ^+ and ϕ^0. Finally, we expect another front to appear which should also propagate into the unstable state ϕ^0 but starts in the lower maximum. This front is represented by the green dotted line and is shown in figure 1.7(d). Furthermore, at $\mu = \mu_c$ this front is a flat solution and thus its velocity is $v = 0$.
The potential is tilted in opposite directions for μ being positive or negative, respectively. Thus when crossing $\mu = 0$ the blue solid front becomes a green dotted front and vice versa.

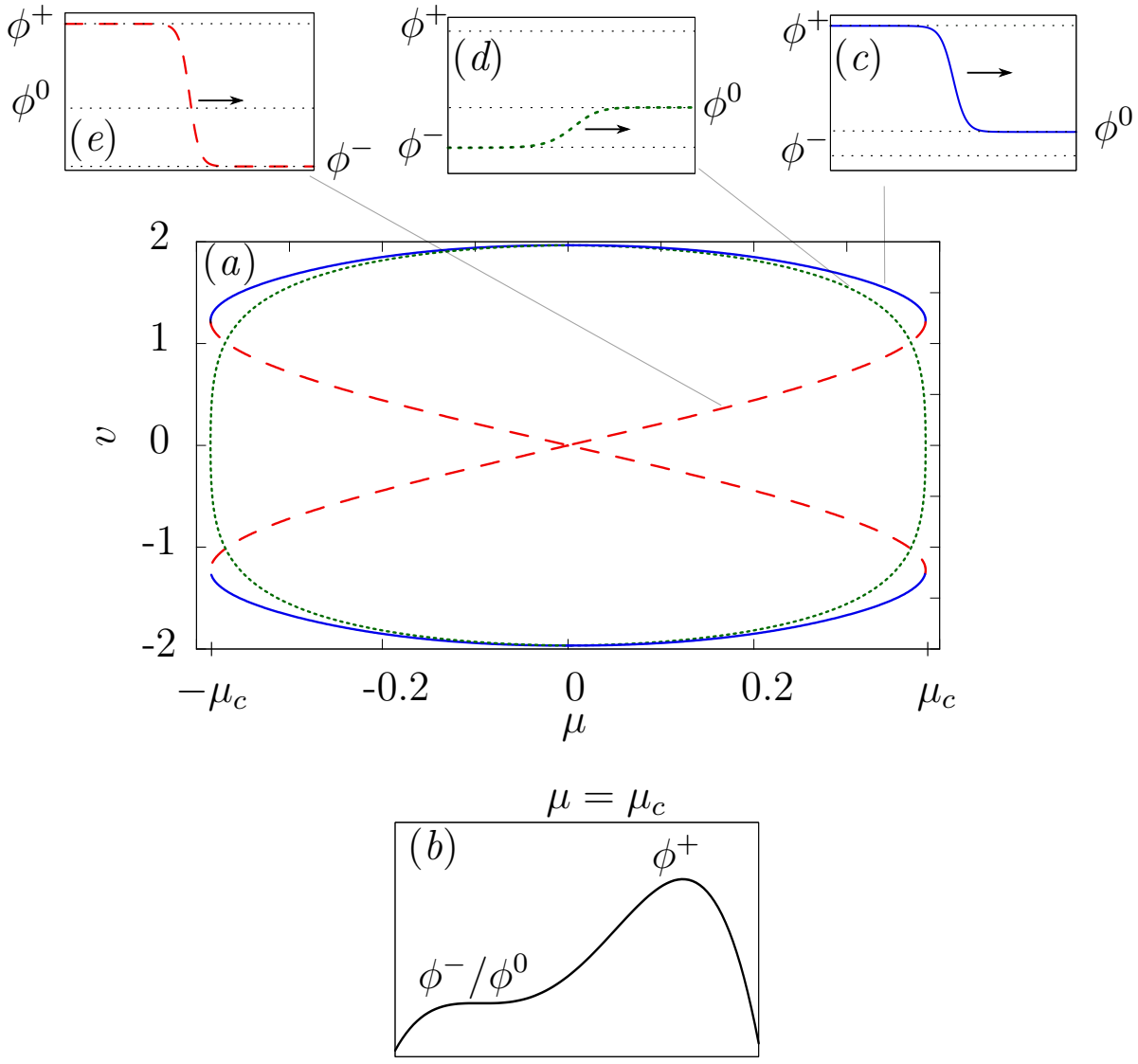

Figure 1.7: In (a) we find the bifurcation diagram for the cubic Allen-Cahn equation (1.47). The red dashed line in the bifurcation diagram represents front solutions between the maxima of the potential in the mechanical analogon. Such a front is depicted in (e). In (b) we see the mechanical potential for $\mu = \mu_c$, where the lower maximum and minimum of the potential merge. In the bifurcation diagram this point is reached, where the red dashed line and the solid blue line merge. Now the front between the two maxima (red) develops into a front between the higher maximum and the minimum (blue), which is depicted in (c). Moreover, there exists another front which connects the minimum and the lower maximum. This solution belongs to the green dotted branch in the bifurcation diagram and an example profile is shown in (d).
When crossing $\mu = 0$ the front between ϕ^0 and ϕ^- becomes the front connecting ϕ^+ and ϕ^0 and vice versa. The arrows denote the direction of motion in the laboratory frame.

What is already striking, is that we have two different front velocities for the propagation into the same unstable state (blue and green). However, we determined only one linear marginal velocity, which only depends on the unstable state. This seems to contradict with our numerical results. Therefore, we firstly examine which of the two possible branches corresponds to the linear marginal velocity. In figure 1.8 the analytically determined linear marginal velocity (1.51) is depicted as the black dashed line. The analytical result fits to the numerically (gregy solid) determined branch, which is equal to the green dotted line in figure 1.7(a). Hence, there must be another front velocity for a front propagating into the unstable state which is illustrated by the blue solid curve in figure 1.7(a).
The other front velocity is called nonlinear marginal velocity which is driven by the nonlinearities of (1.47). Therefore, the next section deals with the theory of the nonlinear marginal stability analysis.

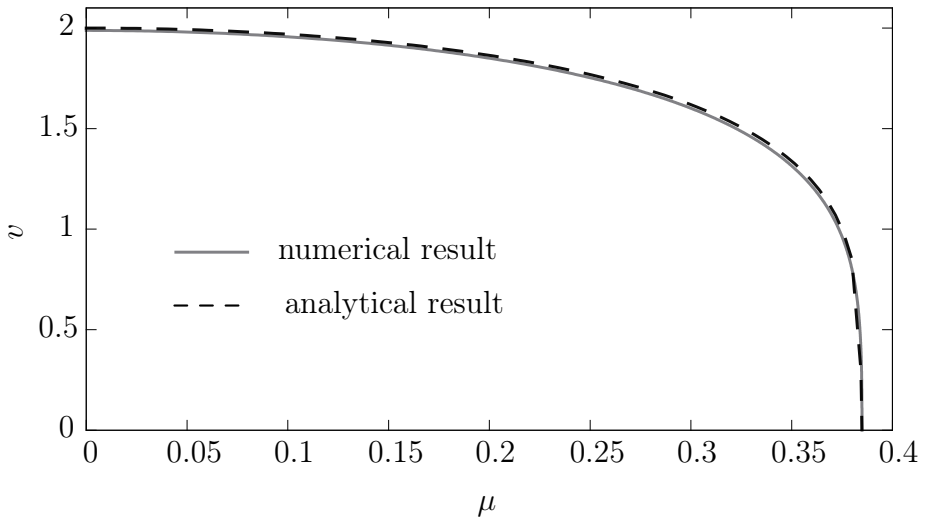

Figure 1.8: The numerical results depicted as grey solid line are in agreement with the analytical linear results illustrated by the black dashed line.

1.5. Nonlinear marginal stability analysis

To understand where the blue solid line in figure 1.7(a) comes from, we first have to understand the idea of nonlinear marginal stability analysis.
If we focus on the asymptotic behavior in the leading edge in the comoving frame and expand ϕ into

$$\phi \sim C_1(v)\mathrm{e}^{-k_1\xi} + C_2(v)\mathrm{e}^{-k_2\xi} + \ldots \qquad \text{with} \quad k_1 < k_2 < \ldots, \tag{1.55}$$

we find that it is dominated for $\xi \to \infty$ by the smallest wave vector k^r, say k_1^r. Thus, $C_1(v)$ needs to be nonzero. We briefly discussed this in section 1.2 and

therefore argued to only focus on the solid branch in figure 1.5.
However, if $C_1 = 0$ for a special $v = v_{nl}$, the asymptotic behavior is dominated by the next smallest wave vector $k_2^r > k_1^r$.
In section 1.2 we found that the linear marginal front velocity is described by the minimum in figure 1.5. Thus, in order to satisfy stability v_{nl} needs to be greater than v_l. Furthermore, the minimum of $v(k^r)$ belongs to the greatest wave vector on the solid branch. As the wave vector corresponding to the nonlinear front is greater than the one for the linear marginal front profile, we now have a solution on the dashed branch as depicted in figure 1.9 by the black dot.

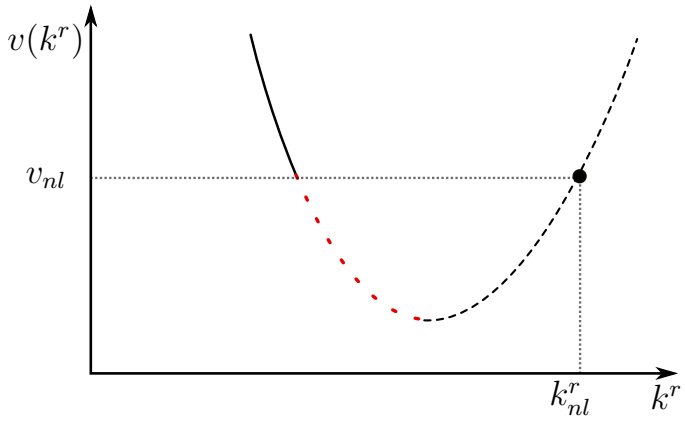

Figure 1.9: The nonlinear marginal velocity is depicted by the black dot on the black dashed line, as it belongs to the wave vector $k_{nl}^r > k_l^r$. All solutions with smaller velocity are unstable, illustrated by the red dotted line. Note that all other stable solutions correspond to the black solid line, as the asymptotic behavior of the leading edge is dominated by the smallest occurring wave vector.

Because, the occurring front is faster and steeper than the linear marginal front, this nonlinear marginal front will invade the profile as depicted in figure 1.10.
Again, any front moving with a slower velocity than v_{nl} will be unstable as illustrated in figure 1.9 by the red dotted line. Accordingly the black dot in figure 1.9 is the point where the front changes its stability and is called the nonlinear marginal stability point. Moreover, following our arguments all other relevant stable solutions belong to the solid black branch in figure 1.9 as the asymptotic behavior is always dominated by the smallest occuring wave vector.

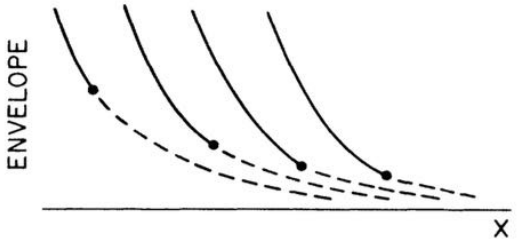

Figure 1.10: The black solid line illustrates the invasion mode with steeper wave vector k_{nl}^r and faster velocity v_{nl} than the linear marginal front profile illustrated by the black dashed line[4].

So, we examined what happens if $C_1\,(v_{nl}) = 0$ which leads us to the question how to figure out when this special case occurs. As the name already suggests we need to focus on the whole nonlinear equation. Hence, we can not offer a general solution for any nonlinear equation but we have to focus on the particular equations and have to find solutions of those. However, it is possible to show, that uniformly translating fronts $\phi(x - vt)$ with $v = v_{nl}$ are marginal stable as presented in the appendix of [7]. We recover shortly their results, as there are small mistakes in the original. Consider the general differential equation:

$$\phi_t = g(\phi, \phi_{xx})\,. \tag{1.56}$$

For a stationary solution ϕ^s in the comoving frame ($\xi = x - vt$) we have:

$$-v\frac{\mathrm{d}\phi^s}{\mathrm{d}\xi} = g(\phi^s, \phi^s_{\xi\xi})\,. \tag{1.57}$$

Consider now perturbation in ϕ^s

$$\phi = \phi^s + \varphi(\xi)\mathrm{e}^{\Omega t}\,, \tag{1.58}$$

and insert this into (1.56). Linearizing g around ϕ^s we obtain

$$\Omega\varphi - v\frac{\mathrm{d}\varphi}{\mathrm{d}\xi} = g_\phi(\phi, \phi_{\xi\xi})\Big|_{\phi=\phi^s}\varphi + g_{\phi_{\xi\xi}}(\phi, \phi_{\xi\xi})\Big|_{\phi=\phi^s}\varphi := L\varphi\,, \tag{1.59}$$

where $g_{\phi_{\xi\xi}}$ denotes the derivative of g with respect to $\phi_{\xi\xi}$, analogously for g_ϕ. L is a linear operator in ϕ^s. Furthermore, for large ξ, say the leading edge we expand

[4]Figure is taken from [17]

ϕ^s and φ into series:

$$\phi^s = \sum_j C_j \mathrm{e}^{-K_j^r \xi} \quad , \qquad 0 < K_j^r < K_{j+1}^r \tag{1.60a}$$

$$\varphi = \sum_j B_j \mathrm{e}^{-k_j^r \xi} \quad , \qquad 0 < k_j^r < k_{j+1}^r \tag{1.60b}$$

We require φ to fall off faster than ϕ^s as the perturbations need to be sufficiently localized, thus $K_1^r < k_1^r$. In the appendix of [17] a counting argument is presented, which shows the existence of front solutions for any $v > v_l$ for the linear analysis. Together with the fact, that (1.59) is linear in φ as for the analysis of the linear velocity, it follows that there exists one $\Omega^*(v)$ with $v > v_l$ such that $B_1 = 0$ (as any solution is possible).
Besides, when deriving (1.57) with respect to ξ we obtain

$$J\left(\frac{\mathrm{d}\phi^s}{\mathrm{d}\xi}\right) = 0 \tag{1.61}$$

$$\text{with} \qquad J := -v\frac{\mathrm{d}}{\mathrm{d}\xi} - L\,. \tag{1.62}$$

Comparing (1.61) with (1.59) we find, that for $\Omega = 0$

$$\varphi = \frac{\mathrm{d}\phi^s}{\mathrm{d}\xi} \tag{1.63}$$

$$\Rightarrow k_j^r = K_j^r \quad \text{and} \quad B_j = -k_j^r C_j \tag{1.64}$$

Accordingly, when the eigenfunction with $B_1 = 0$ coincides with the translational mode $\Omega = 0$ we have $C_1 = 0$ which is exactly what happens when $v = v_{nl}$. However, this implies that stability changes at $v = v_{nl}$ because we have $\Omega = 0$. Thus, if $v = v_{nl}$ the corresponding front profile is marginal stable.
Nevertheless, we can only show for each particular differential equation that a profile with velocity greater than v_{nl} will eventually approach the nonlinear velocity.
Finishing the theoretical arguments concerning linear and nonlinear marginal stability analysis we would like to note that the linear marginal stable front and the nonlinear marginal stable front are often also referred to as pulled and pushed front, respectively. Pulled fronts are dominated by the behavior of the leading edge and therefore are pulled along by the tip of the front. Contrarily, pushed fronts follow from the interior nonlinearities of the front and thus, are pushed ahead by the nonlinear part or the previously mentioned invasion mode.
In [9] the nonlinear fronts are described as 'strongly heteroclinic' connections in the phase space, as they leave the unstable state in the phase space along the

strongly stable eigendirection.
Moreover, in [8] the difference between a linear and a nonlinear front is defined by introducing and studying different type of stabilities and examining the occurring stable solutions in parameter space. Besides, they also regard the phase space in order to understand the defined stabilities and instabilities.

1.6. Nonlinear marginal stability analysis of the Allen-Cahn equation

In this section we study the whole nonlinear Allen-Cahn equation in the comoving frame

$$-v\frac{\mathrm{d}\phi}{\mathrm{d}\xi} = \frac{\mathrm{d}^2\phi}{\mathrm{d}\xi^2} + \phi - \phi^3 + \mu\,, \tag{1.65}$$

to find the solution of fronts corresponding to the blue solid line in figure 1.7. We follow here the ideas given in [12], [7] and [13].
The fronts run between the states ϕ^+, ϕ^- and ϕ^0. We write ϕ^s to denote one of the two stable states. Because the front is monotonic we define

$$h(\phi) = \frac{\mathrm{d}\phi}{\mathrm{d}\xi}\,. \tag{1.66}$$

In order to satisfy the Neumann boundary conditions we request

$$h\left(\phi^0\right) = h\left(\phi^s\right) = 0\,. \tag{1.67}$$

Deriving (1.66) with respect to ξ yields

$$\frac{\mathrm{d}\phi}{\mathrm{d}\xi}\frac{\mathrm{d}h}{\mathrm{d}\phi} = h(\phi)\frac{\mathrm{d}h}{\mathrm{d}\phi} = \frac{\mathrm{d}^2\phi}{\mathrm{d}\xi^2}\,. \tag{1.68}$$

Thus, inserting (1.66) and (1.68) into (1.65) we get:

$$-vh(\phi) = h(\phi)\frac{\mathrm{d}h}{\mathrm{d}\phi} + \phi - \phi^3 + \mu\,. \tag{1.69}$$

Furthermore, we form the power series ansatz up to second order

$$h(\phi) = a_0 + a_1\phi + a_2\phi^2\,. \tag{1.70}$$

With the requirement (1.67) we obtain

$$a_0 + a_1\phi^s + a_2(\phi^s)^2 = 0 \tag{1.71a}$$
$$a_0 + a_1\phi^0 + a_2(\phi^0)^2 = 0\,. \tag{1.71b}$$

Applying the Gauss-method, further leads to

$$\begin{aligned} a_1(\phi^s-\phi^0) &= -a_2\left(\phi^s-\phi^0\right)\left(\phi^s+\phi^0\right) \\ &\Rightarrow a_1 := a_2 c \qquad \text{with} \quad c=-\left(\phi^s+\phi^0\right) && \text{(1.72a)} \\ a_0 &= -a_1\phi^s - a_2(\phi^s)^2 = a_2\left(\phi^s+\phi^0\right)\phi^s - a_2(\phi^s)^2 \\ &\Rightarrow a_0 = a_2\phi^0\phi^s := a_2 b \qquad \text{with} \quad b=\phi^0\phi^s && \text{(1.72b)} \\ \Rightarrow \quad h(\phi) &= a_2\left(\phi^0\phi^s-\left(\phi^0+\phi^s\right)\phi+\phi^2\right) = a_2\left(b+c\phi+\phi^2\right). && \text{(1.72c)} \end{aligned}$$

Inserting (1.72c) into (1.69) and comparing the coefficients of each order in ϕ leads to

$$\begin{aligned} -va_2\left(b+c\phi+\phi^2\right) &= a_2^2\left(b+c\phi+\phi^2\right)(c+2\phi)+\phi-\phi^3+\mu && \text{(1.73a)} \\ \phi^0: \qquad -va_2 b &= a_2^2 bc+\mu && \text{(1.73b)} \\ \phi^1: \qquad -va_2 c &= 2a_2^2 b+a_2^2 c^2+1 && \text{(1.73c)} \\ \phi^2: \qquad -va_2 &= 3a_2^2 c \Rightarrow \quad v=3a_2(\phi^0+\phi^s) && \text{(1.73d)} \\ \phi^3: \qquad 0 &= 2a_2^2-1 \Rightarrow \quad a_2=\pm\frac{1}{\sqrt{2}}. && \text{(1.73e)} \end{aligned}$$

This is an overdetermined system of equations. However, we can show graphically that (1.73b) and (1.73c) are satisfied when inserting (1.73d)[5]. Note, that if we considered higher order in ϕ in (1.70) the coefficient comparison would always return a polynomial up to second order. Thus, we obtain an exact solution to the cubic Allen-Cahn equation with

$$\begin{aligned} v(\mu) &= \frac{3}{\sqrt{2}}\left(\phi^0+\phi^+\right) \\ &= \sqrt{6}\left(\cos\left(\frac{1}{3}\arccos\left(\frac{3\sqrt{3}}{2}\mu\right)\right)-\cos\left(\frac{1}{3}\arccos\left(\frac{3\sqrt{3}}{2}\mu\right)+\frac{\pi}{3}\right)\right), \end{aligned} \tag{1.74}$$

as the velocity for a front propagating from ϕ^+ into ϕ^0.
In figure 1.11 the analytical nonlinear velocity (1.74) is depicted (black dashed line) in comparison with the numerical results (grey solid line) obtained with *auto-07p*. When μ is negative, the mechanical potential is tilted such that the nonlinear front connects ϕ^0 and ϕ^-. By changing ϕ^+ to ϕ^- in (1.74) we get the corresponding front velocities. We find, that the analytical nonlinear result fits perfectly to the numerical result in the interval $0.2078 < |\mu| < \frac{2}{3\sqrt{3}} \approx 0.3849$[6]. However, the results

[5] See appendix A.1
[6] See calculation of crossing point in the appendix A.2

differ for $|\mu| < 0.2078$.

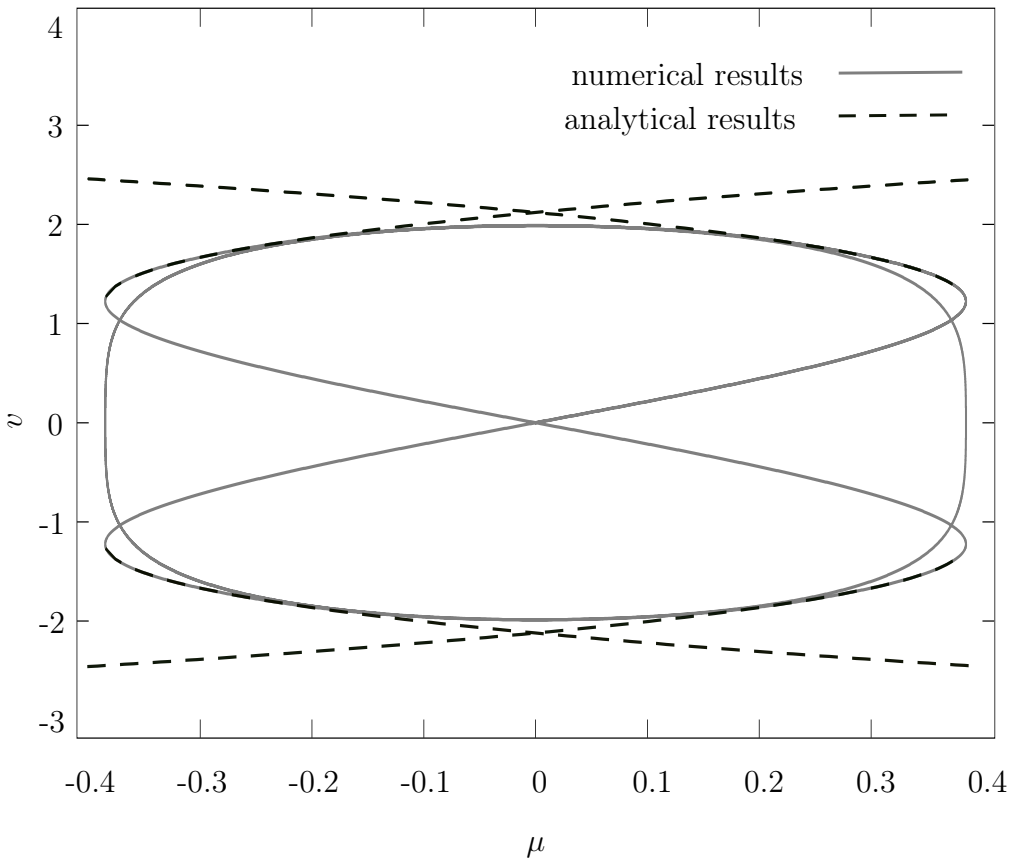

Figure 1.11: The numerical results depicted as grey solid line are in agreement with the analytical results illustrated by the black dashed line. However, only for $0.2078 < |\mu| < \frac{2}{3\sqrt{3}}$.

In order to understand the behavior around $\mu = 0.2078$ we need to examine the wave vector in the asymptotic behavior, following the idea of section 1.5. Therefore, we determine the front solution by integrating[7] (1.66):

$$\phi(\xi) = \frac{1}{2}|\phi^0 - \phi^s| \tanh\left(-\frac{1}{2\sqrt{2}}|\phi^0 - \phi^s|\xi\right) + \frac{1}{2}(\phi^0 + \phi^s)\,. \tag{1.75}$$

The asymptotic behavior $\xi \to \infty$ of the $\tanh(k\xi)$ is dominated by the mode $\mathrm{e}^{-2k\xi}$.

[7] See appendix A.3

Thus, the asymptotic wave vector k^r_{nl} for $\mu \geq 0$ is:

$$\begin{aligned} k^r_{nl}(\mu) &= \frac{1}{\sqrt{2}}|\phi^0 - \phi^+| \\ &= \sqrt{\frac{2}{3}}\left|\cos\left(\frac{1}{3}\arccos\left(\frac{3\sqrt{3}}{2}\mu\right)\right) + \cos\left(\frac{1}{3}\arccos\left(\frac{3\sqrt{3}}{2}\mu\right) + \frac{\pi}{3}\right)\right| \end{aligned} \tag{1.76}$$

Figure 1.12 (left) shows the linear marginal wave vector k^r_l and the nonlinear marginal wave vector k^r_{nl} depending on μ. The right panel gives the corresponding velocities v_l and v_{nl}. For $\mu < 0.2078$ we find $k^r_{nl} < k^r_l$ and $v_{nl} > v_l$. Thus, these solutions correspond to the solid branch in figure 1.5 and therefore, the linear marginal velocity is selected. However, as $\mu > 0.2078$ we have $k^r_{nl} > k^r_l$ and $v_{nl} > v_l$ which is exactly the case discussed in the previous section and illustrated in figure 1.9 by the dot on the dashed branch.
Note, that here we have two different front types, which is why the linear marginal velocity still exists for $\mu > 0.2078$.

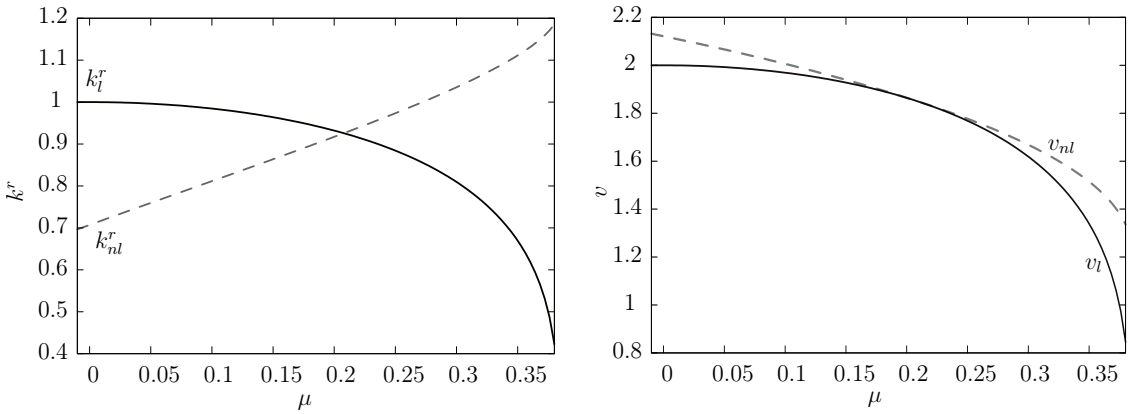

Figure 1.12: Left: Wave vector k^r_l and k^r_{nl} of the linear and nonlinear marginal analysis, respectively.
Right: The linear marginal velocity v_l and the nonlinear marginal velocity v_{nl}.
For $\mu < 0.2078$, k^r_{nl} is smaller but v_{nl} is greater than the characteristics for the linear analysis. Hence, for $\mu < 0.2078$, the linear marginal velocity is selected for both fronts, but for $\mu > 0.2078$ the nonlinear marginal velocity occurs for the front between the states ϕ^0 and ϕ^+.

Similarly to the previous analysis we can determine the velocity of a front between ϕ^+ and ϕ^-. Remembering the mechanical analogon, we find that only one front velocity is possible, as the particle can only move from one hill to the other with

one particular friction. Hence the velocity is analogously to (1.74)

$$\begin{aligned} v_s(\mu) &= \frac{3}{\sqrt{2}}\left(\phi^- + \phi^+\right) \\ &= \sqrt{6}\left(\cos\left(\frac{1}{3}\arccos\left(\frac{3\sqrt{3}}{2}\mu\right) - \frac{\pi}{3}\right) - \cos\left(\frac{1}{3}\arccos\left(\frac{3\sqrt{3}}{2}\mu\right) + \frac{\pi}{3}\right)\right), \end{aligned} \tag{1.77}$$

and the corresponding solution is

$$\phi(\xi) = \frac{1}{2}|\phi^- - \phi^+|\tanh\left(-\frac{1}{2\sqrt{2}}|\phi^- - \phi^+|\xi\right) + \frac{1}{2}(\phi^- + \phi^+)\,. \tag{1.78}$$

Now, we can compare the analytical results with those obtained with *auto-07p*. To compare the results, we examine the derivatives of the front profiles as possible differences appear clearer.
In figure 1.13(a), (b) and (d) we compare the numerical results for the fronts' derivatives (red solid line) with the determined analytical results (black dashed line) and find that they are in agreement. However, in panel (b) at $\mu = 0.0$ for the front propagating into the unstable state, we compare the derivative gained with *auto-07p* with the analytical nonlinear marginal result. The latter corresponds to the analytical solution point in the bifurcation diagram in figure 1.11 where the two black dashed branches cross each other at $\mu = 0$. As we can not compute analytically a front profile for a front moving with the linear marginal velocity, we can only compare the solutions corresponding to the crossing point of the black dashed branches with the solution of the grey solid line at $\mu = 0$ and $v = 2.0$ in figure 1.11. The modulus derivative in figure 1.13(c) corresponding to the numerical result (linear marginal) is greater than the modulus derivative corresponding to the analytical result (nonlinear marginal). Hence, the linear marginal profile is steeper than the nonlinear marginal front profile. This is again in agreement with our argument (compare fig. (1.12)).

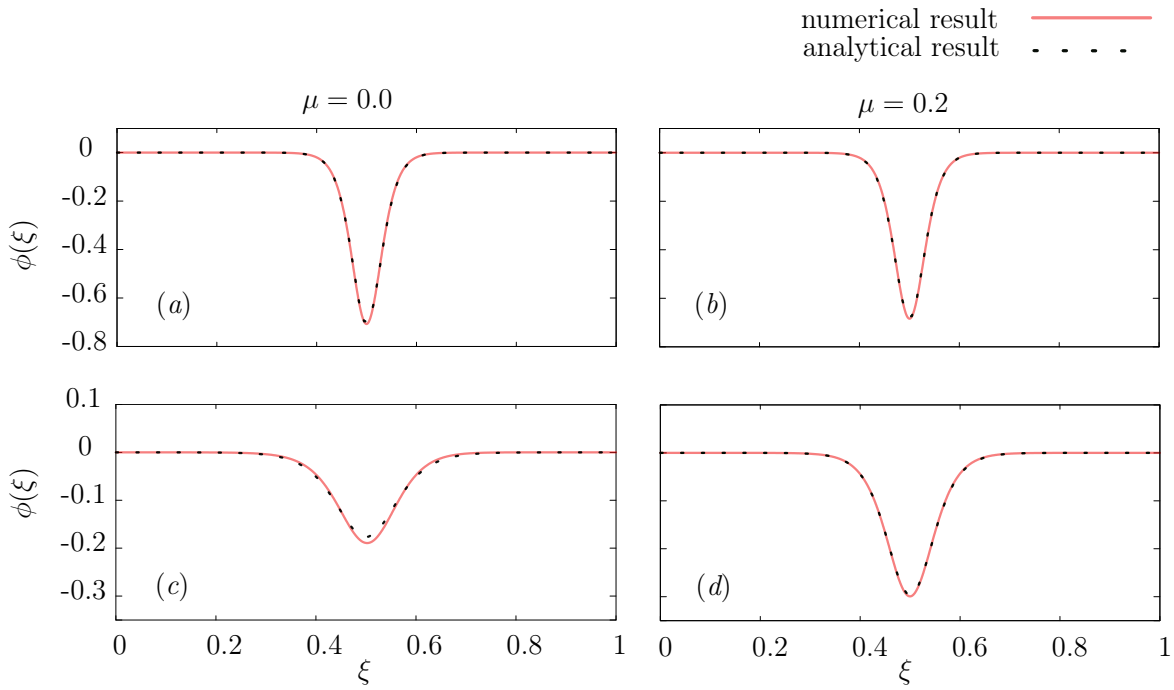

Figure 1.13: Comparison of numerical (red solid line) and analytical (black dashed line) derivative of front solutions for four different fronts.
(a): Front between the two stable states for $\mu = 0.0$
(b): Front between the two stable states for $\mu = 0.2$.
(c): Front between the stable and unstable state for $\mu = 0.0$. Here the black dashed line corresponds to the derivative of the nonlinear marginal solution which is why the results differ. However, this is in agreement with our theory.
(d): Front between the stable and the unstable state for $\mu = 0.2$.

In the previous section we referred to the nonlinear marginal solution as an invasion mode. In order to understand this behavior we implemented a finite difference method together with a four step Runge-Kutta method to examine the time evolution of front solutions. At $\mu = 0.377$ consider a front solution composed of a front between ϕ^+ and ϕ^- together with a front propagating from ϕ^- into ϕ^0 at time $t = 0$ as depicted in figure 1.14 (left) with the solid line. At a later time $t = 1$ this front has evolved into a direct front between ϕ^+ and ϕ^0 (dotted line in the right panel). Examining figure 1.7(a) we find in the region between the bifurcation point where the red dashed and solid blue branches merge and the point where the red dashed line crosses the green dotted line[8], so for $0.3730 \leq |\mu| \leq \mu_c$, that $v_{nl} \geq v_s > v_l$. Hence, for the initial composed front the part between the two stable states catches up with the linear marginal part until the latter finally vanishes. The new occurring front is the nonlinear front between ϕ^+ and ϕ^0 moving with

[8]See calculation of this crossing point in the appendix A.2

v_{nl}. Thus, the front between the two stable states acts as an invasion mode close to the bifurcation point at $\mu = \mu_c$. At the bifurcation point this front merges into the nonlinear marginal front.

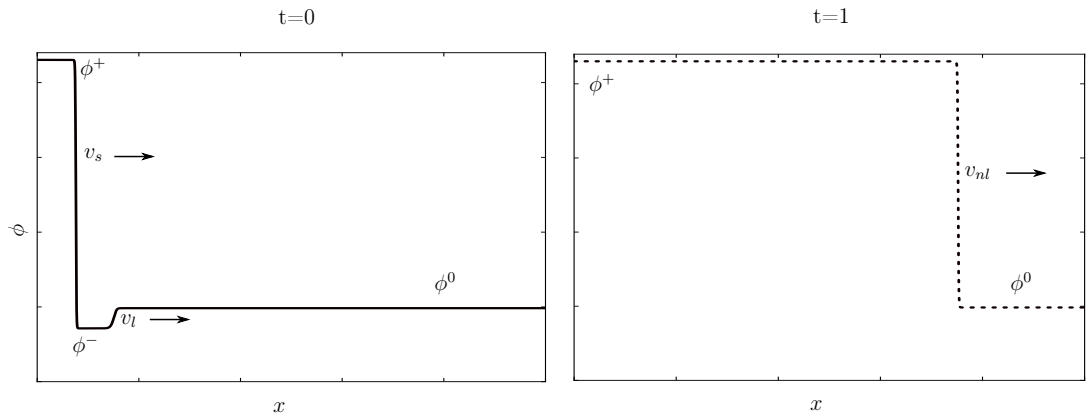

Figure 1.14: Results of direct numeric time evolution. The black solid line on the left is a profile composed of a front between the two stable states and the linear marginal front. At a later time t this fronts evolves into the nonlinear marginal front depicted on the right as the dotted line.

Additionally, we present space-time plots in figure 1.15 to exemplify the behavior of the invasion mode. Therefore we study a front composed of a front from ϕ^+ into ϕ^- and a front propagating from ϕ^- into the unstable state ϕ^0. We implemented again a finite-difference method and chose a point in the leading edge (of the corresponding parts in the front profile) to study its space-time behavior. We neglect labelling the t and x axis as we are interested in the qualitative results. The slope of the lines in the space-time plot equal the velocity of the point in the respective leading edge. Hence, the steeper the slope, the faster the front. In figure 1.15 on the left we show a space-time plot for $\mu = 0.350$. Considering the bifurcation diagram depicted in figure 1.7 the crossing point of the green dotted and the red dashed branches is at $\mu = 0.3730$. Thus, for $\mu = 0.350$ $v_l > v_s$ and the distance between two different front profiles diverges. This implies, that the red dashed line never crosses the green dotted line in figure 1.15 on the left. However, at $\mu = 0.375$ we have $v_l < v_s < v_{nl}$ (see fig. 1.7(a)) and thus, a front composed of the linear marginal and the front between the two stable states evolves into the nonlinear marginal front. The green dotted line crosses the red dashed line and the whole front now moves faster, as the blue solid line is steeper than the green and the red line in figure 1.15 on the right. The slope of each line in figure 1.15

is indeed in agreement with the quantitive velocity values found in the bifurcation diagram in figure 1.7.

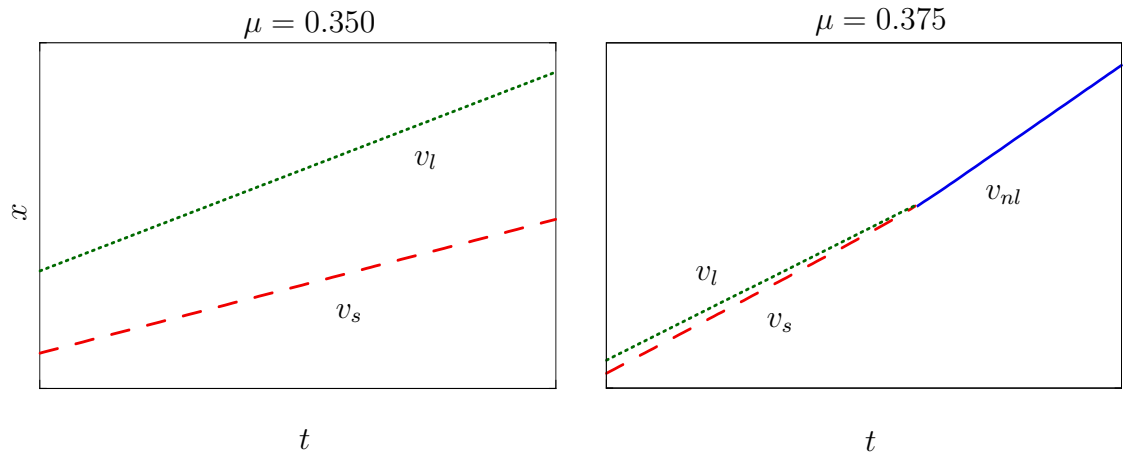

Figure 1.15: Space-time plots of the cubic Allen-Cahn system. The slope of the lines represents the velocity of a point in the leading edge of the corresponding front profile.
Left: At $\mu = 0.350$ the linear marginal velocity v_l is greater than the velocity v_s of a front between ϕ^+ and ϕ^-. Therefore, the green dotted line is steeper than the red dashed line and both never cross each other. In the front profile composed of these two fronts an increasing plateau at ϕ^- evolves.
Right: At $\mu = 0.375$, $v_l < v_s < v_{nl}$ and therefore a composed front eventually moves with the nonlinear marginal velocity, as the green dotted and the red dashed line cross each other and a new steeper solid blue line evolves, which corresponds to the nonlinear marginal velocity.

So far, we showed that the nonlinear velocity is marginally stable but we also need to show that any front with a velocity greater than v_{nl} converges towards the marginal stability point. However, we have not yet found a way to study this nonlinear behavior analytically.

2. The quintic Allen-Cahn equation

In this section we study an equation similar to the one examined in Bechhoefer et al. [6]. First, we will recover what has been determined in this paper in order to motivate the equation we are studying here.

2.1. Reproduction of the Bechhoefer et al. paper

The paper by Bechhoefer et al. deals with an Allen-Cahn-type equation with a local energy density up to fifth order in ϕ

$$\begin{aligned} \frac{\partial \phi}{\partial t} &= \frac{\partial^2 \phi}{\partial x^2} - f'(\phi) \\ f'(\phi) &= \phi(\phi - (0.5 - b))(\phi - 1)(\phi - 1.5)(\phi - 2)\,. \end{aligned} \tag{2.1}$$

The stable states are 0, 1 and 2 whereas the unstable states are 1.5 and $0.5 - b$. To stay consistent with the interval in the previously studied system we shift the energy density such that the stable states are at $\phi_s^- = -1$, $\phi_s^0 = 0$ and $\phi_s^+ = 1$ and the unstable states are at $\phi_u^+ = 0.5$ and $\phi_u^- = -0.5 - b$:

$$f'(\phi) = \phi(\phi + (0.5 + b))(\phi + 1)(\phi - 0.5)(\phi - 1)\,. \tag{2.2}$$

The control parameter b changes the position of the unstable state and thus the value of the energy density at $\phi_s^- = -1$. In the mechanical analogon this means, that the height of the very left hill in the inset of figure 2.1 changes by varying b. Consider $\phi_s^- = -1$ as a liquid phase, $\phi_s^0 = 0$ as quasicrystal phase and $\phi_s^+ = 1$ as a solid phase. The paper deals with the creation of a macroscopically large region of the metastable[9] state. Therefore, they examine the three possible front velocities between the particular stable states. We recover their results with *auto-07p* which is depicted in figure 2.1.

[9] we refer to the metastable states as the state which never corresponds to the global minimum of the free energy density f, namely ϕ_s^0.

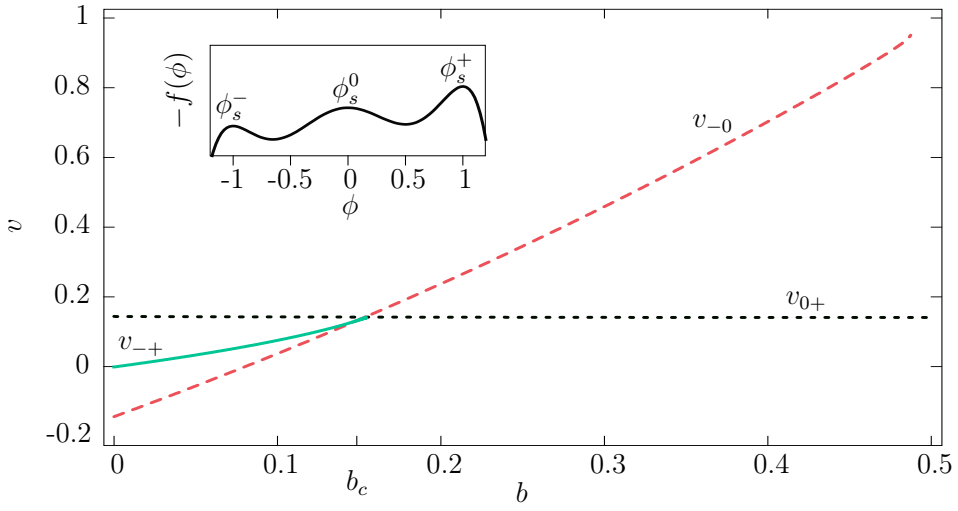

Figure 2.1: Velocities for different possible fronts between the three stable states depending on the control parameter b. The mechanical potential is depicted in the inset for $b = b_c \approx 0.154$

Because $f(\phi_s^0)$ and $f(\phi_s^+)$ do not change with the control parameter b, the front velocity v_{0+} (black dotted line) between these two states is constant over b. The speed of the front propagating from ϕ_s^0 into ϕ_s^- is increasing with b (red dashed line). However, what is striking is that a front moving from ϕ_s^+ into ϕ_s^- does not exist for $b > b_c = 0.15419$ as the green solid line for v_{-+} ends at b_c in a heteroclinic bifurcation. Regarding the structure of the potential in the mechanical analogon, we find that the velocities v_{-0} and v_{0+} are independent of each other. But v_{-+} relates to both velocities. As the hill at ϕ_s^+ is higher than the one at ϕ_s^0 we need a sufficient friction for a particle moving from one to the other. Besides, if the particle moves from ϕ_s^+ to ϕ_s^- this friction needs to be lower in order to pass the hill at ϕ_s^0. Thus we obtain: $v_{-+} < v_{0+}$. Moreover, considering a particle starting at ϕ_s^- more negative friction is needed to reach ϕ_s^+ than it is to reach ϕ_s^0. This yields: $v_{-+} > v_{-0}$. As v_{-0} and v_{0+} are independent, their branches in figure 2.1 may cross. However, v_{-+} always needs to satisfy the discussed relations and thus can not exist for $b > b_c$.

At the crossing point we have $v_{-+} = v_{-0} = v_{0+}$ as depicted in figure 2.2. We can always imagine an approximate front between ϕ_s^+ and ϕ_s^- being composed of a front between ϕ_s^- and ϕ_s^0 and a front between ϕ_s^0 and ϕ_s^+. Thus, the front profile shows a plateau at ϕ_s^0. When decreasing b, the rear part catches up with the leading part such that the system propagates directly from ϕ_s^+ into ϕ_s^- and a nonlinear velocity for the front exists. On the other hand, by increasing b the leading part moves ahead such that the plateau at ϕ_s^0 becomes wider and wider and no velocity exists such that a front between ϕ_s^+ and ϕ_s^- would rest in a frame

moving with such a velocity. In other words, increasing b such that $b > b_c$ means that a direct transition from the liquid phase into the solid phase is impossible. However, a macroscopically large region of the metastable state is created. As b represents the temperature of the system, control of this parameter allows us to create a macroscopic quantity of the quasicrystalline phase.

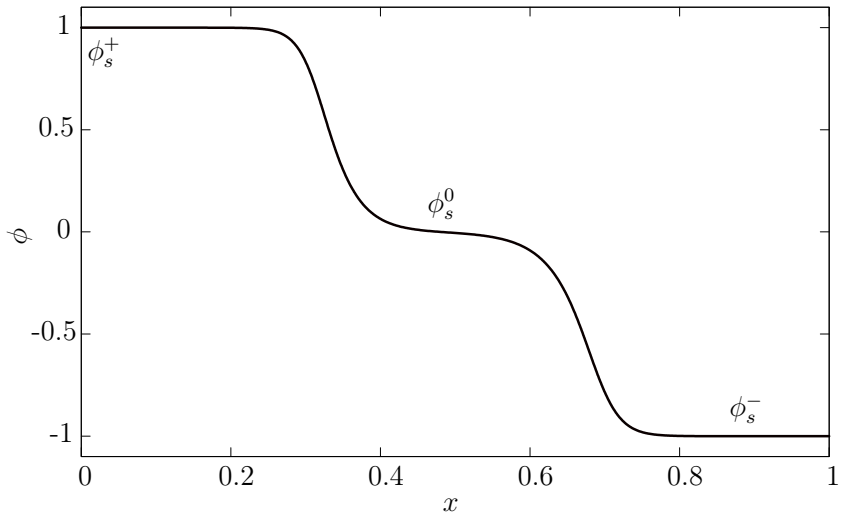

Figure 2.2: Front solution at $v_{-+} = v_{-0} = v_{0+}$ for $b = b_c$ on the green solid line in figure 2.1. The front shows a plateau at ϕ_s^0 which increases when increasing b.

We presented here, the idea of the paper but we would like to comment, that throughout their argument Bechhoefer et. al. never mention the interaction between two fronts when composing a front of two possible solutions. However, due to the nonlinearities this interaction occurs and influences the width of the plateau at ϕ_s^0. This is also the reason why the plateau's width of the front profile in figure 2.2 at $b = b_c$ does not converge. At $b = b_c$ the three branches in figure 2.1 cross, hence there still exists a solution for the propagation of ϕ_s^+ into ϕ_s^- and this solution has a certain width due to the interaction caused by the nonlinearities. However, for $b > b_c$ such a front can not exist. We refer to [12] where the interaction of two similar fronts (with different direction of motion) is calculated analytically. However, we can not transfer this to the system discussed here, as the two fronts are different which makes the analysis more difficult or even impossible. We do not determine the interaction either analytically or numerically and leave this as an outlook for further research.

2.2. Continuation in μ and v for the quintic Allen-Cahn equation

In the following instead of parameter b we employ again the chemical potential μ as main control parameter. In particular, we use:

$$\begin{aligned} -v\frac{\partial\phi}{\partial x} &= \frac{\partial^2\phi}{\partial x^2} - f'(\phi) \\ f'(\phi) &= \phi(\phi+0.5)(\phi+1)(\phi-0.5)(\phi-1) - \mu = \phi^5 - 1.25\phi^3 + 0.25\phi - \mu\,. \end{aligned} \tag{2.3}$$

Remember that we start for the Allen-Cahn equation in *auto-07p* by continuing in the domain-size L. Therefore, we sinusoidally perturb the unstable state $\phi^0 = 0$ and increase the domain size L at fixed μ, such that a front between the two stable states develops. We let the velocity v adapt, however during this first continuation v remains at zero, as at $\mu = 0$ the front between the two stable states in the Allen-Cahn equation does not move. Regarding now the Bechhoefer et al. equation at $\mu = 0$ we further have the two unstable states $\phi_u^+ = 0.5$ and $\phi_u^- = -0.5$. Thus, perturbing either of these unstable states results in a front between the metastable state ϕ_s^0 and ϕ_s^+ and between ϕ_s^0 and ϕ_s^-, respectively. However, as the local free energy density f is different at ϕ_s^0, ϕ_s^+ and ϕ_s^-, the velocity of such a front is $v \neq 0$. For reasons we do not understand yet *auto-07p* does not adapt the velocity but stops the continuation (even if we start with a small velocity $v \neq 0$). Moreover, with this method we can not find all possible front solutions of the system. This is why we start in *auto-07p* with three free different local energy densities f which are in a limiting case identical or similar to the one for the cubic Allen-Cahn equation (which we already implemented in *auto-07p*):

$$f_1'(\phi) = -0.5\phi - 1.5\phi^2 - \phi^3 + b(-\phi^5 + 0.25\phi + 1.5\phi^2 + 2.25\phi^3) + \mu \tag{2.4a}$$

$$f_2'(\phi) = \phi - \phi^3 + b(-\phi^5 - 1.25\phi + 2.25\phi^3) + \mu \tag{2.4b}$$

$$f_3'(\phi) = -0.5\phi + 1.5\phi^2 - \phi^3 + b(-\phi^5 + 0.25\phi - 1.5\phi^2 + 2.25\phi^3) + \mu\,. \tag{2.4c}$$

For $b = 0$ and $\mu = 0$ the corresponding mechanical potentials are illustrated in figure 2.3. As we are only interested in the position of the extrema we neglect the values on the f-axis for simplification. We now start in *auto-07p* perturbing each of the unstable states in f_1, f_2 and f_3. Thus, we obtain front profiles at $v = 0$ between the two stable states, respectively. Next, we continue in μ and v for $b = 0$ and in all three cases this results in qualitatively identical bifurcation diagrams as for the cubic Allen-Cahn equation, shown in figure 1.7(a).

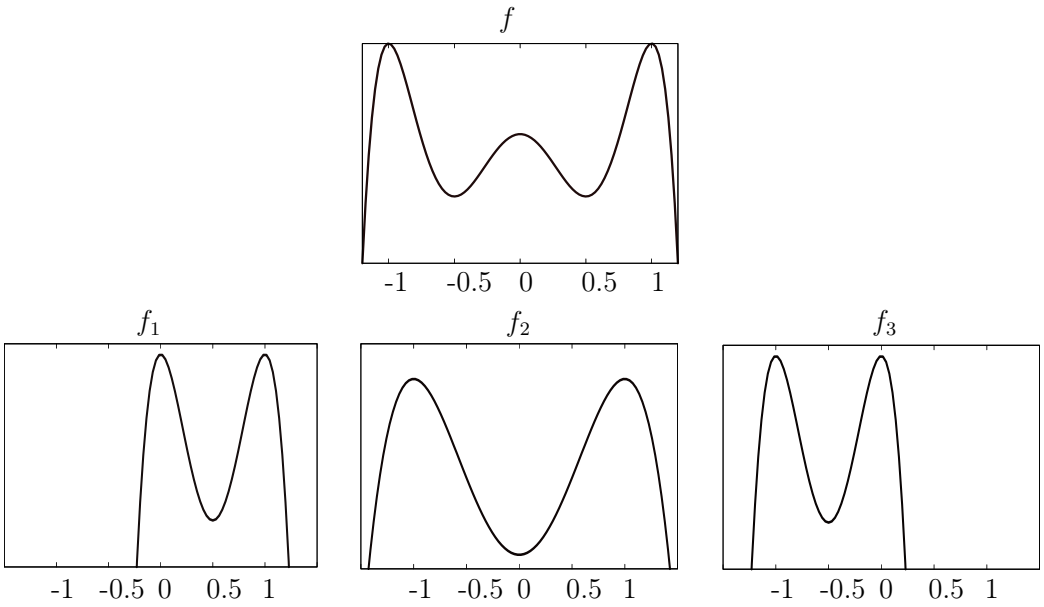

Figure 2.3: All possible transitions in the mechanical potential corresponding to f for $\mu = 0$ in (2.3) can be found regarding three double-well Allen-Cahn potentials f_1, f_2 and f_3 with different stable and unstable states for $b = 0$.

We recall, that for the Allen-Cahn equation with $\mu = 0$ fronts between the unstable state $\phi^0 = 0$ and the stable states $\phi^+ = 1$ and $\phi^- = -1$ as well as fronts between the two stable states occur. Therefore, we first continue in μ and v for f_1, f_2 and f_3 and then increase b up to $b = 1$ for the different front solutions obtained at $\mu = 0$. At this value we obtain $f' = f_1' = f_2' = f_3'$. Thus, we obtain 3 different starting points to continue again in μ and v and obtain the whole bifurcation diagram for Eq. (2.3), which is depicted in figure 2.4(a). The three different starting points are the points at $\mu = 0$ and $v \geq 0$ where the red solid lines, the orange dotted lines and the grey dot-dashed lines cross.

In the following, we explain the front solutions corresponding to the different branches in figure 2.4(a). Therefore, we first examine the behavior of f when varying μ. Two special cases are illustrated in the panels (b) and (c) in figure 2.4. First, for $\mu = \mu_{c1} \approx 0.044$ the metastable state ϕ_s^0 merges with the unstable state ϕ_u^+. Similarly, for $\mu = -\mu_{c1}$, ϕ_s^0 and ϕ_u^- merge. Increasing μ further, we end up at $\mu_{c2} \approx 0.114$ where ϕ_s^- and ϕ_u^- merge. Hence, for $\mu > \mu_{c2}$ no fronts can occur. Again, for $\mu = -\mu_{c2}$, ϕ_s^+ and ϕ_u^+ merge.

Let us now consider the different branches in the bifurcation diagram and the corresponding front solutions:

The red solid branches correspond to fronts between the two stable states ϕ_s^- and ϕ_s^+ as exemplarily shown in panel (d). Because both states exist for the whole

range of μ, the red branches bifurcate into the blue dashed branches at $|\mu| = \mu_{c2}$. At this point the stable states merge with the unstable states, as mentioned above. So, the blue dashed branches correspond to fronts between ϕ_s^+ and ϕ_u^- or between ϕ_s^- and ϕ_u^+, depending on the sign of μ. This is exemplarily shown in panel (e). We examine the behavior of this front in more detail below. We obtained the red and blue branches by considering the front between the two stable states in f_2 at $\mu = v = 0$.

On the other hand, studying the differential equation with f_1 yields for $\mu = 0$ the velocity for a front between $\phi = 0$ and $\phi = 1$. Increasing b and then again continue in μ and v results in the orange dotted branches. Along these branches fronts between the stable states ϕ_s^+, ϕ_s^- and the metastable state ϕ_s^0 occur. One possible solution is illustrated in panel (f) in figure 2.4. We study exemplarily the behavior of the corresponding solution branch in order to understand the evolution of all orange branches. So, we have a front propagating into the metastable state ϕ_s^0 as the velocity is positive. Increasing μ from zero, the branch crosses $v = 0$ and thus the direction of the front is changed. Regarding the illustrated mechanical potentials we can understand this behavior: By increasing μ the 'hill' at ϕ_s^- decreases in height whereas the one at ϕ_s^0 increases. However, the velocity is determined by the difference in energy density values indicated by Eq. (1.11). Thus, the sign changes, when the 'hills' are of equal height. Moreover, the branch ends at $\mu = \mu_{c1}$ as ϕ_s^0 vanishes for greater μ.

Following the same branch by decreasing μ, a new, green solid branch bifurcates at $\mu = -\mu_{c1}$. Here the two states ϕ_u^- and ϕ_s^0 merge and thus the front propagates from ϕ_s^- into ϕ_u^-. This is shown in panel (g). The front exists for $-\mu_{c1} < \mu < \mu_{c2}$. At $\mu = \mu_{c2}$ the two connected states merge and the front profile becomes flat which corresponds to $v = 0$.

There is only one other front-type left, which is illustrated by the grey dot-dashed lines. These fronts are generated by taking the transition from $\phi = 0$ the unstable state $\phi = \pm 0.5$ in f_1 or f_3 increasing b and again continue in μ and v. In panel (h), we find such a front solution. The corresponding solution branch exists for $-\mu_{c1} < \mu < \mu_{c1}$. At $\mu = -\mu_{c1}$ the two states ϕ_u^- and ϕ_s^0 merge. Therefore, the front profile becomes flat and $v = 0$. On the other hand, for $\mu > \mu_{c1}$ the front vanishes, as ϕ_s^0 vanishes. As we argued previously, at the $\mu \neq 0$ value corresponding to the crossing point of the two orange dotted branches the hills in the mechanical potential $f(\phi_s^-) = f(\phi_s^0)$ (or $f(\phi_s^-) = f(\phi_s^0)$) are of equal 'height', hence the linear marginal velocities of the front profiles corresponding to the green solid and the grey dot-dashed branches are equal.

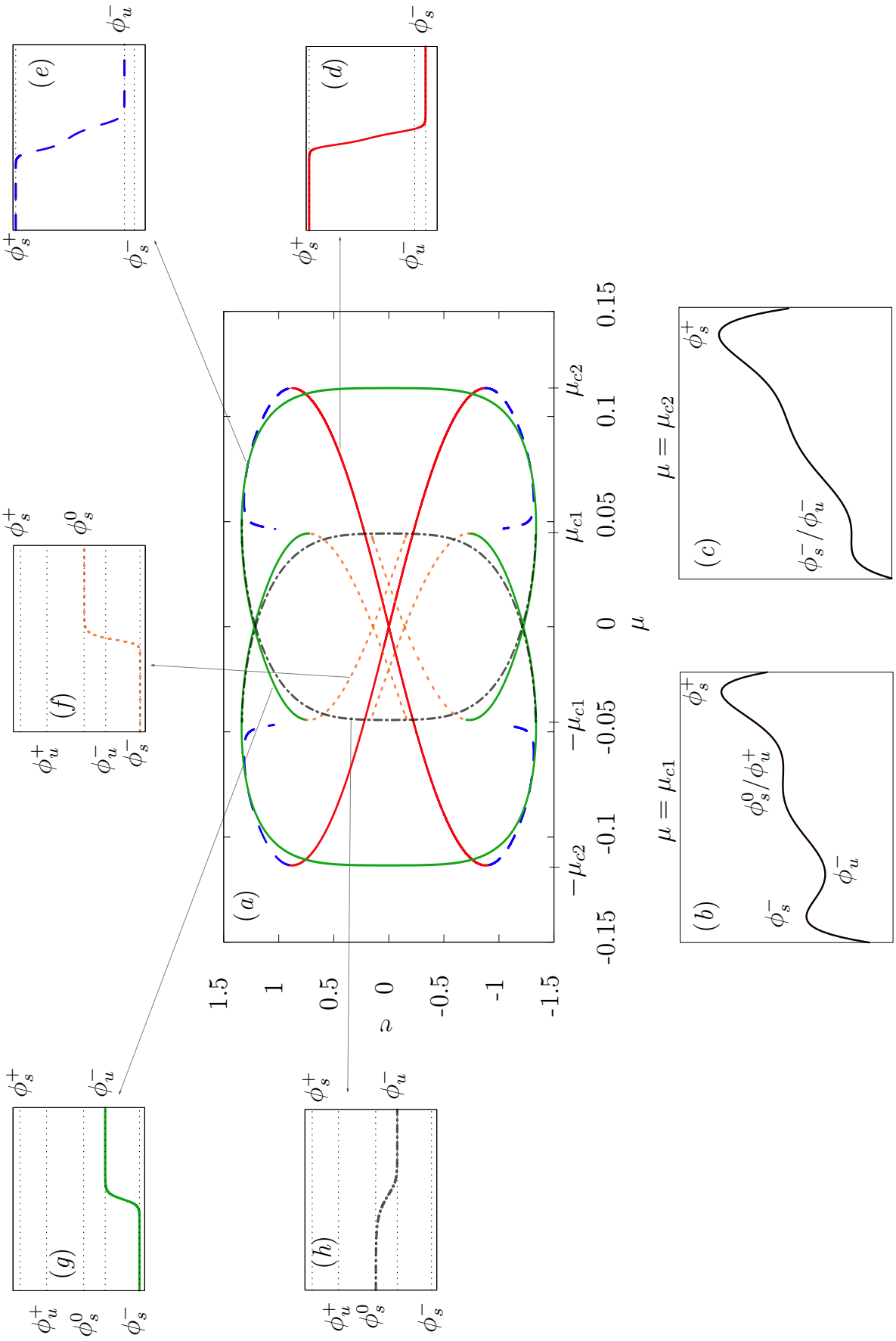
(a)
(b)
(c)
(d)
(e)
(f)
(g)
(h)
u
μ
μ_{c2}
μ_{c1}
$-\mu_{c1}$
$-\mu_{c2}$
$\mu = \mu_{c1}$
$\mu = \mu_{c2}$
ϕ_s^+
ϕ_s^0
ϕ_s^-
ϕ_u^+
ϕ_u^-
ϕ_s^0/ϕ_u^+
ϕ_s^-/ϕ_u^-

Figure 2.5: Bifurcation diagram for front solutions of the quintic Allen-Cahn equation employed by Bechhoefer et al. [6]. The red solid branches correspond to fronts between the two stable states ϕ_s^+ and ϕ_s^-, as depicted in panel (d). At the bifurcation point $\mu = \mu_{c2}$ the states ϕ_s^- and ϕ_u^- merge. This is also depicted in the mechanical potential in (c). Because these states merge, the front evolves into a front between ϕ_s^+ and ϕ_u^-, represented by the blue dashed branch and shown in panel (e).
The green solid branches correspond to fronts between ϕ_s^- and ϕ_u^- or ϕ_s^+ and ϕ_u^+ depending on the sign of μ. However, at the critical value of $\mu = \mu_{c1}$ the states ϕ_s^0 and ϕ_u^+ merge (for $\mu = -\mu_{c1}$ the states ϕ_s^0 and ϕ_u^- merge). The corresponding mechanical potential is illustrated in (b). Thus, the green solid front solution presented in panel (g), changes into the orange dotted front solution depicted in (f). Hence, the orange dotted branches refer to front solutions between ϕ_s^+ and ϕ_s^0 or ϕ_s^- and ϕ_s^0, again depending on the sign of μ.
Finally, the grey dot-dashed lines represent front solutions between ϕ_s^0 and ϕ_u^+ or between ϕ_s^0 and ϕ_u^-. An exemplarily profile is shown in panel (h). At the critical value μ_{c1} these fronts become flat solutions and therefore satisfy $v = 0$. The black dotted lines in the panels for the front profiles represent the homogenous roots of (2.5).

Because

$$-\phi^5 + 1.25\phi^3 - 0.25\phi + \mu = 0\,, \tag{2.5}$$

is a quintic function we are not able to determine the roots for any μ analytically. Therefore, we can not calculate the stable states of the system for any μ. Nevertheless, (2.5) can be solved numerically with *auto-07p* by continuing in μ. Consequently, we are able to study the linear marginal velocity by inserting the numerical results into:

$$v_{l+} = \pm 2\sqrt{-f''(\phi_u^+)} = \pm 2\sqrt{-5\phi_u^{+4} + 3.75\phi_u^{+2} - 0.25} \tag{2.6}$$

$$v_{l-} = \pm 2\sqrt{-f''(\phi_u^-)} = \pm 2\sqrt{-5\phi_u^{-4} + 3.75\phi_u^{-2} - 0.25}\,, \tag{2.7}$$

where v_{l+} is the linear marginal velocity for a front invading the unstable state ϕ_u^+ and v_{l-} corresponds to a front invading the state ϕ_u^-. The linear marginal results are depicted in figure 2.6 as the black dashed line for v_{l-} and the black dot-dashed line for v_{l+}. The results obtained with *auto-07p* are indicated by the grey solid lines and in part coincide with the semi-analytical results.

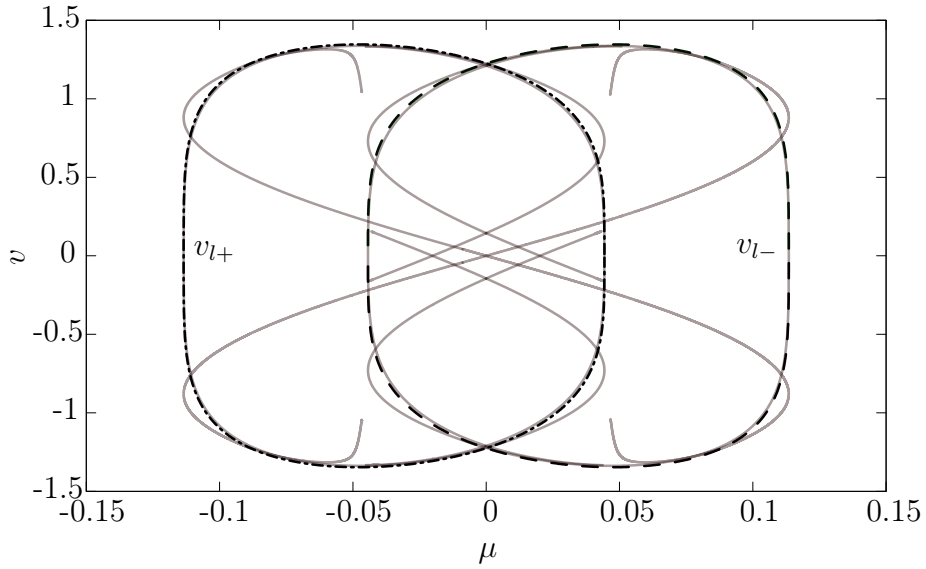

Figure 2.6: The linear marginal velocity v_{l-} corresponds to the black dashed line whereas v_{l+} corresponds to the black dot-dashed line. The results gained with *auto-07p* are illustrated as the grey solid lines.

So, we discover that the grey dot-dashed branches as well as the green solid branches (only for $|\mu| > \mu_{c1}$) in figure 2.4(a) correspond to fronts moving with the linear marginal velocity. We can not make the same ansatz as in Eq. (1.66) and develop h into a power series, as this power series does not converge for Eq.

(2.3). In order to understand, which branches belong to the nonlinear front velocities, we study symmetries of the bifurcation diagram. Thus, we notice that the bifurcation diagram for the simple cubic Allen-Cahn equation (Fig. 1.7(a)) qualitatively occurs again within the whole bifurcation diagram (Fig. 2.4(a)). The red solid branches over the whole μ-range together with the blue dashed and the green solid line for $|\mu| > \mu_{c1}$ show a similar structure. Therefore, we expect the blue dashed branch to correspond to a nonlinear marginal front, because we can identify these fronts as invasion modes (analogously to section 1.6) at the bifurcation point, where it merges with the red branch. Moreover, regarding the interval $-\mu_{c1} < \mu < \mu_{c1}$ we observe the structure for the cubic Allen-Cahn equation twice. We motivate this again referring to the mechanical analogon: In the particular interval we can consider the potential as being composed of two Allen-Cahn potentials, namely f_1 and f_2, depicted in figure 2.3. At the critical value $|\mu| = \mu_{c1}$ the metastable state merges with either one of the unstable states and thus the two Allen-Cahn potentials are no longer separated from each other. So, the mid point of the Allen-Cahn structure corresponding to f_1 and f_3 within the whole bifurcation diagram, is the point where $v = 0$ and the two orange dotted branches cross. Again, this is in line with our argument, as at this point $f(\phi_s^+) = f(\phi_s^0)$ or $f(\phi_s^-) = f(\phi_s^0)$. Hence, we deduce that in this interval the green solid branch belongs to the nonlinear marginal front solutions. This can also be shown by studying a front being composed of an orange dotted front and a grey dashed dotted front around the bifurcation point $|\mu| = \mu_{c1}$. Such a front evolves into a green solid front solution, as this front invades the system. This is analog to what we studied in section 1.6. The behavior is depicted in figure 1.14.
Let us now return to the blue dashed front. In order to understand why the front vanishes for $|\mu| < \mu_{c1}$ we need to study again the mechanical analogon at $\mu = \mu_{c1}$ in panel (b) in figure 2.4. Consider a particle starting at ϕ_s^+ and ending in ϕ_u^- without overshooting. Let the corresponding friction be v_1. Regard now a particle that moves from ϕ_s^+ to ϕ_s^0, the according friction v_2 needs to satisfy $v_2 > v_1$. Moreover, a particle starting in ϕ_u^- requires more negative friction to move up to ϕ_s^+ than it does to move up to ϕ_s^0. Hence, we claim $v_1 > v_3$, where v_3 is the friction to move from ϕ_s^0 to ϕ_u^-. So, we require $v_3 < v_1 < v_2$, where v_3 corresponds to the velocity at μ_{c1} of the grey dot-dashed branch $v_3 \approx 1.33$. However, v_2 belongs to the velocity at the bifurcation point, where the orange dotted branch becomes the green solid branch with $v_2 \approx 0.73$ which is less than v_3. Hence, v_1, the velocity of the blue dashed solution does not satisfy the condition at $\mu = \mu_{c1}$ and therefore, vanishes. The question arising is: Where exactly does the branch end? Because

the front is expected to be a nonlinear marginal front, it needs to satisfy $v_{nl} > v_l$, which it does not at $|\mu| = \mu_{c1}$. However, we assume these front solutions to appear due to finite-size and boundary effects. The bifurcation diagram in figure 2.4(a) corresponds to a domain size $L = 82$ which is the maximum we could generate. In figure 2.7 the bifurcation diagram for $L = 50$ is illustrated where we emphasized the blue dashed branch corresponding to the discussed front solution. What is already striking, is the existence of front solutions for $|\mu| < \mu_{c1}$ which contradicts our previous argument. However, regarding the illustrated front solution in the inset for $\mu \approx \mu_{c1}$ we find that at the right boundary the unstable state ϕ_u^- (corresponding to the homogenous solution of (2.5)) is not reached anymore. So again, in the mechanical analogon this would imply that the particle moves into the state ϕ_u^- with an overshoot, as the blue dashed line crosses the homogenous state. This overshoot is not detected in *auto-07p* and thus not depicted in the solution. However, the numerical solution must be unstable as the marginal front is the one that directly ends in ϕ_u^- without overshooting. Thus, the solutions obtained with *auto-07p* for a domain size $L = 50$ are not a good representation of the limit $L \to \infty$.

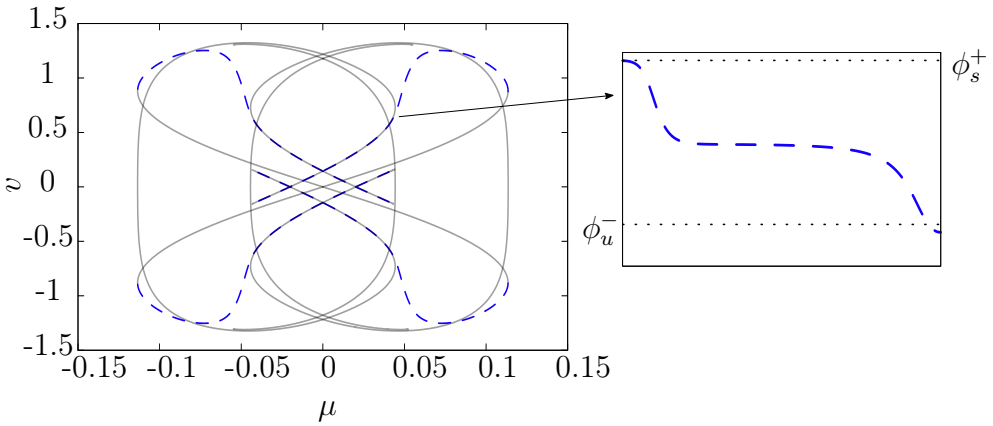

Figure 2.7: On the left: Bifurcation diagram for domain size $L = 50$. The blue dashed lines correspond to the nonlinear fronts.
On the right: Front profile at $\mu \approx \mu_{c1}$ the dotted horizontal lines correspond to the homogenous solutions of Eq. (2.5).

Therefore, we assume the blue dashed branch in figure 2.4 to merge into the green solid branch and end there. Thus, the solutions obtained with *auto07p* which correspond to the part of the branch that satisfy $v < v_l$ would be unstable.
We can conclude that the analysis with *auto-07p* needs to be improved by finding a way to increase the domain size in order to fully understand the behavior of the system.

3. Non-variational cubic Allen-Cahn equation

3.1. Velocity of a front for the non-variational cubic Allen-Cahn equation

So far, we examined variational Allen-Cahn-type equation, i.e. variational implies that the time evolution is determined by a functional derivative of a free energy functional. In section 1.1 we determined the velocity for fronts in the variational cubic Allen-Cahn equation, i.e.

$$v = \pm \frac{f\left(\phi^i\right) - f\left(\phi^f\right)}{\int_{-\infty}^{\infty} \left(\frac{\mathrm{d}\phi}{\mathrm{d}\xi}\right)^2 \mathrm{d}\xi}\,, \tag{3.1}$$

and found that it depends on the difference in local energy densities of the two states the front connects. In this section we add a non-variational term g_{nv} to the simple cubic Allen-Cahn equation (1.47). We follow the idea given in [11] and write

$$\frac{\partial \phi}{\partial t} = \frac{\partial^2 \phi}{\partial x^2} + \phi - \phi^3 + \mu + \epsilon g_{nv}\left(\phi, \frac{\partial \phi}{\partial x}, \frac{\partial^2 \phi}{\partial x^2}\right) \tag{3.2}$$

$$\text{with} \qquad g_{nv}\left(\phi, \frac{\partial \phi}{\partial x}, \frac{\partial^2 \phi}{\partial x^2}\right) = \left(\frac{\partial \phi}{\partial x}\right)^2 + 2b\phi \frac{\partial^2 \phi}{\partial x^2}\,. \tag{3.3}$$

Note, that for $b = 1$, g_{nv} is variational with the functional [10]

$$G = \int \phi \left(\partial_x \phi\right)^2 \mathrm{d}x\,. \tag{3.4}$$

We are interested in the velocity of a front for a non-variational problem and if and how the dependence on the difference in energy densities changes. Therefore, we study the front profile between the two stable states. Hence, we introduce the ansatz

$$\phi(x,t) = \phi_F(x - vt) + u(x - vt, \epsilon t) \qquad \text{with} \quad v = v_0 - \epsilon v_1\,, \tag{3.5}$$

where ϕ_F is the solution (1.78) to the variational cubic Allen-Cahn equation with velocity v_0, i.e.

$$-v_0 \frac{\partial \phi_F(\xi)}{\partial \xi} = \frac{\partial^2 \phi_F(\xi)}{\partial \xi^2} + \phi_F(\xi) - \phi_F(\xi)^3 + \mu \qquad \text{with} \quad \xi = x - v_0 t\,. \tag{3.6}$$

[10] The functional derivative of G needs to be added to (1.1) in order to obtain the equation of motion for ϕ

Note, that with the ansatz (3.5) we introduce a shift ϵv_1 of order ϵ in the velocity. This reflects that the velocity changes due to the non-variational term. Moreover, we add a small adjustment function u also of order ϵ. For the ansatz (3.5) we introduce $\zeta = x - vt = \xi + \epsilon v_1 t$. Linearising $\phi_F(\zeta)$ around ξ yields

$$\phi_F(\zeta) = \phi_F(\xi) + \epsilon v_1 \frac{\partial \phi_F}{\partial \zeta}\bigg|_{\zeta=\xi} + \mathcal{O}(\epsilon^2) \tag{3.7}$$

Inserting the ansatz (3.5) into (3.2) using (3.7) and linearizing in ϵ yields

$$\begin{aligned}
&-v_0 \frac{\partial \phi_F}{\partial \zeta}\bigg|_{\zeta=\xi} - \epsilon v_1 v_0 \frac{\partial^2 \phi_F}{\partial \zeta^2}\bigg|_{\zeta=\xi} + \epsilon v_1 \frac{\partial \phi_F}{\partial \zeta}\bigg|_{\zeta=\xi} - v_0 \frac{\partial u}{\partial \zeta} \\
=&\frac{\partial^2 \phi_F}{\partial \zeta^2}\bigg|_{\zeta=\xi} + \epsilon v_1 \frac{\partial^3 \phi_F}{\partial \zeta^3}\bigg|_{\zeta=\xi} + \phi_F\bigg|_{\zeta=\xi} + \epsilon v_1 \frac{\partial \phi_F}{\partial \zeta}\bigg|_{\zeta=\xi} - \phi_F^3\bigg|_{\zeta=\xi} \\
&- 3\epsilon v_1 \phi_F^2 \frac{\partial \phi_F}{\partial \xi}\bigg|_{\zeta=\xi} + \mu + \frac{\partial^2 u}{\partial \zeta^2} + u - 3\phi_F(\xi)^2 u + \epsilon g_{nv}\left(\phi_F(\zeta), \frac{\partial \phi_F}{\partial \zeta}, \frac{\partial^2 \phi_F}{\partial \zeta^2}\right)\bigg|_{\zeta=\xi}.
\end{aligned} \tag{3.8}$$

With (3.6) this further simplifies to

$$\begin{aligned}
&-\epsilon v_1 v_0 \frac{\partial^2 \phi_F}{\partial \zeta^2}\bigg|_{\zeta=\xi} + \epsilon v_1 \frac{\partial \phi_F}{\partial \zeta}\bigg|_{\zeta=\xi} - v_0 \frac{\partial u}{\partial \zeta} \\
=&\epsilon v_1 \frac{\partial^3 \phi_F}{\partial \zeta^3}\bigg|_{\zeta=\xi} + \epsilon v_1 \frac{\partial \phi_F}{\partial \zeta}\bigg|_{\zeta=\xi} - 3\epsilon v_1 \phi_F^2 \frac{\partial \phi_F}{\partial \zeta}\bigg|_{\zeta=\xi} \\
&+ \frac{\partial^2 u}{\partial \zeta^2} + u - 3\phi_F(\xi)^2 u + \epsilon g_{nv}\left(\phi_F(\zeta), \frac{\partial \phi_F}{\partial \zeta}, \frac{\partial^2 \phi_F}{\partial \zeta^2}\right)\bigg|_{\zeta=\xi}.
\end{aligned} \tag{3.9}$$

Deriving (3.6) with respect to ξ

$$-v_0 \frac{\partial}{\partial \xi}\frac{\partial \phi_F(\xi)}{\partial \xi} = \frac{\partial}{\partial \xi}\frac{\partial^2 \phi_F(\xi)}{\partial \xi^2} + \frac{\partial \phi_F(\xi)}{\partial \xi} - 3\phi_F(\xi)^2 \frac{\partial \phi_F(\xi)}{\partial \xi}, \tag{3.10}$$

and introducing the linear operator

$$L = -v_0 \frac{\partial}{\partial \xi} - \frac{\partial^2}{\partial \xi^2} - 1 + 3\phi_F(\xi)^2, \tag{3.11}$$

we obtain

$$L^\dagger\left(\frac{\partial}{\partial \xi}\phi_F(-\xi)\right) = 0, \tag{3.12}$$

where $L^\dagger$ is the adjoint of L. Next, we identify the linear operator (3.11) in (3.9)

$$\epsilon v_1 \frac{\partial \phi_F}{\partial \zeta}\bigg|_{\zeta=\xi} + \epsilon v_1 L\left(\frac{\partial}{\partial \xi}\phi_F\right) + Lu = \epsilon g_{nv}\bigg|_{\zeta=\xi}, \tag{3.13}$$

where we used the fact that $\frac{\partial \xi}{\partial \zeta} = 1$. With (3.12), (3.13) simplifies to

$$Lu = \epsilon g_{nv}\left(\phi_F, \frac{\partial \phi_F}{\partial \xi}, \frac{\partial^2 \phi_F}{\partial \xi^2}\right) - \epsilon v_1 \frac{\partial \phi_F}{\partial \xi} \tag{3.14}$$

According to the Fredholm alternative [21] (3.14) is only solvable if

$$\left\langle \epsilon g_{nv}\left(\phi_F, \frac{\partial \phi_F}{\partial \xi}, \frac{\partial^2 \phi_F}{\partial \xi^2}\right) - \epsilon v_1 \frac{\partial \phi_F}{\partial \xi} \,\middle|\, \frac{\partial}{\partial \xi}\phi_F \right\rangle = 0\,, \tag{3.15}$$

because (3.12) has a nontrivial solution. We employed here that

$$\phi_F(-\xi) = -\phi_F\,, \tag{3.16}$$

hence, the minus sign cancels out in the scalar product in (3.15). Thus, we obtain for the non-variational velocity

$$v_1 = \frac{\int_{-\infty}^{\infty} g_{nv}\left(\phi_F, \frac{\partial \phi_F}{\partial \xi}, \frac{\partial^2 \phi_F}{\partial \xi^2}\right) \partial_\xi \phi_F \,\mathrm{d}\xi}{\int_{-\infty}^{\infty} \left(\partial_\xi \phi_F\right)^2 \,\mathrm{d}\xi}\,. \tag{3.17}$$

So, v_1 no longer depends on the difference in energy densities as in (3.1) but on the non-variational part g_{nv} and the front shape $\partial_\xi \phi$.

3.2. Numerical results for non-variational cubic Allen-Cahn equation

In order to obtain the bifurcation diagram for the non-variational cubic Allen-Cahn equation, we first generate the bifurcation diagram for g_{nv} being variational, i.e. $b = 1$. Therefore, we set the domain size $L = 50$ in *auto07p* and continue as mentioned in the previous sections in L and v. Afterwards we continue in μ and v to obtain the bifurcation diagram for the simple cubic Allen-Cahn equation. This is depicted in figure 3.1 as the grey solid line. Next, we set $\mu = 0$ and $v = 0$ and continue in ϵ and v up to $\epsilon = 0.2$. Eventually, we continue again in μ and v which yields the black dashed bifurcation diagram in figure 3.1.

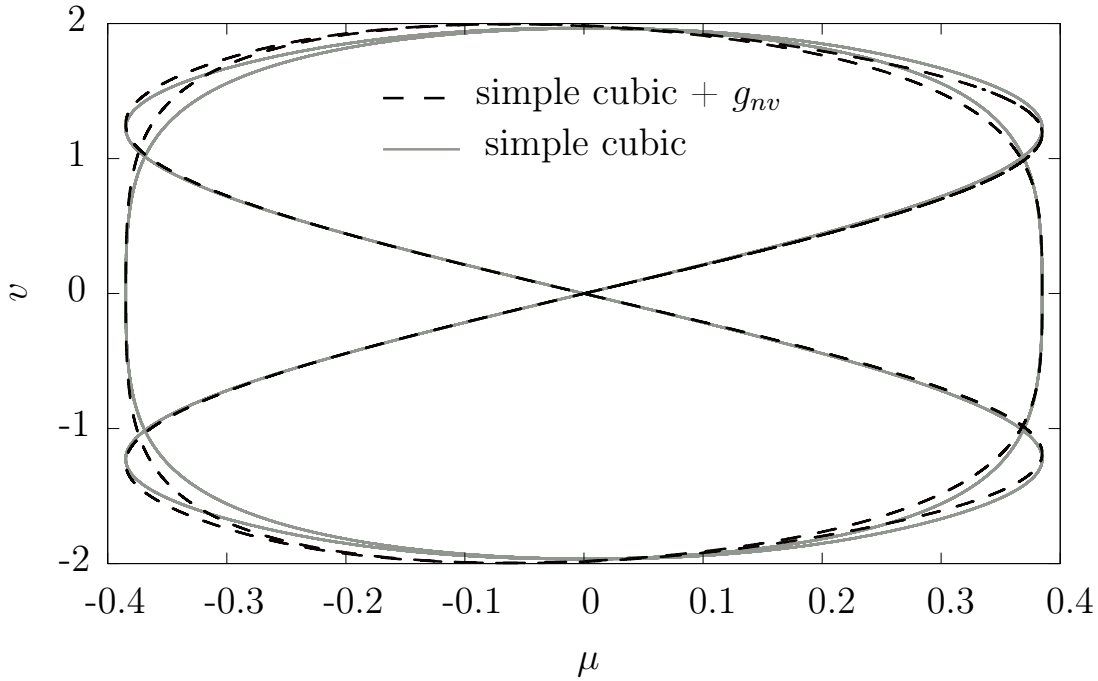

Figure 3.1: Comparison of bifurcation diagrams for the simple cubic Allen-Cahn equation $\epsilon =$ (grey solid) and the cubic Allen-Cahn equation with additional variational term g_{nv}, $\epsilon = 0.2$ and $b = 1$ (black dashed).

Comparing the two bifurcation diagrams we find that the $\mu \to -\mu$ symmetry is broken. This is due to the non-variational term which breaks the $\phi \to -\phi$ symmetry (as it is quadratic in ϕ) and thus also the $\mu \to -\mu$ symmetry. However, for $\mu = 0$ we obtain in both cases $v = 0$ which is in line with our analysis of the previous section. As g_{nv} corresponds to a functional derivative the velocity depends on the difference in energy densities [11] and therefore is zero for $\mu = 0$ in any variational case with symmetric local energy density. Moreover, we find that the diagonal branches through $\mu = 0$ coincide. Thus, we can conclude with (3.1) that for a front between the stable states the term $\frac{\mathrm{d}\phi}{\mathrm{d}\xi}$ does not differ when adding the variational term. This is in contrast to a front propagating into the unstable state as the bifurcation diagrams differ clearly when adding g_{nv} with $b = 1$. As the corresponding velocity also satisfies equation (3.1) and as the numerator does not change[12] we deduce that $\frac{\mathrm{d}\phi}{\mathrm{d}\xi}$ changes for fronts into the unstable state when adding the variational term g_{nv}.

Now, we change b to $b = 2$ and continue again in μ and v. In figure 3.2 the corresponding bifurcation diagram is depicted (black dashed line) compared to the previously determined bifurcation diagram for $b = 1$ (grey solid line). The

[11] We refer to A.4 in the appendix for the explicit determination of v for (3.2) with $b = 1$
[12] See appendix A.4

symmetry $\mu \to -\mu$ is broken and the difference increases with increasing b. As the equation of motion is no longer variational a shift in the velocity ϵv_1 appears. Therefore, at $\mu = 0$ the velocity differs from zero as what is in contrast to the variational case. Inserting ϕ_F from Eq. (1.78) into (3.17) and solving the integrals[13] for $\mu = 0$ yields

$$v_1 = \frac{2\sqrt{2}}{5}. \tag{3.18}$$

Hence, we obtain employing (3.5) a shift in the velocity

$$-\epsilon v_1 = -0.2\frac{2\sqrt{2}}{5} \approx -0.11 \tag{3.19}$$

for a front propagating from $\phi^+ = 1$ into $\phi^- = -1$ at $\mu = 0$. This shift is indicated in red in figure 3.2 and indeed coincides with the numerical result.

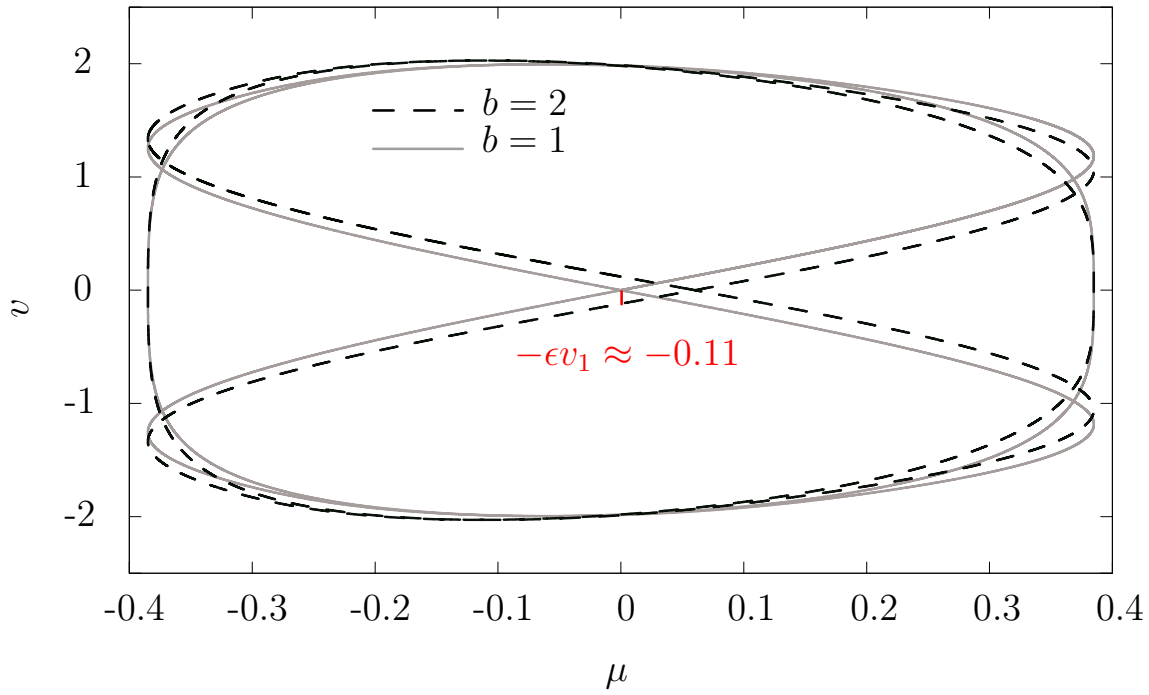

Figure 3.2: Comparison of bifurcation diagrams for the variational cubic Allen-Cahn equation with $b = 1$ (grey solid) and the non-variational cubic Allen-Cahn equation with $b = 2$ (black dashed). The red line indicates the shift in velocity v_1 for a front propagating from ϕ^+ into ϕ^- at $\mu = 0$.

Note, that we can also insert (1.78) for all possible μ into (3.17). However, the integrals become more difficult and we neglect to solve them analytically but leave this as an outlook.

[13] See appendix A.5

4. Conclusion and outlook

In this thesis we examined Allen-Cahn-type equations, the occurring front profiles and the corresponding front velocities. Therefore, we introduced the linear marginal stability analysis, which focuses on the leading edge of the front. Thus, one can linearize the equation of motion and determine the velocity v_l employing the dispersion relation $\omega(k^r)$. However, we found a second front, propagating into the same unstable state with velocity $v_{nl} > v_l$ for the cubic Allen-Cahn equation. We obtained the corresponding front profile using the so called nonlinear marginal stability analysis. This front is no longer pulled along by the leading edge but now pushed ahead by the nonlinearities, therefore, we need to study the whole nonlinear equation. Our analytical results for the cubic Allen-Cahn equation are in line with our numerical results obtained with the continuation program *auto07p*. We also showed the time evolution of a so called invasion mode in order to show the formation of the nonlinear front.
Moreover, we studied a quintic Allen-Cahn equation, for which we are not able to find an analytical solution. Therefore, we determined numerically the homogenous steady states and inserted them into the analytical formula for the linear marginal velocity. Thus, we were able to figure out the branches in the bifurcation diagram corresponding to the linear marginal velocities. In order to find the branches corresponding to the nonlinear fronts we compared the bifurcation diagram for the quintic with the one for the cubic Allen-Cahn equation using symmetry arguments for the invasion mode. In the final section we examined a non-variational cubic Allen-Cahn equation and determined analytically the shift in velocity for a front between the two stable states at $\mu = 0$. Our analytical and numerical results coincide.
However, we were not able to show analytically that any front profile with a velocity $v > v_{nl}$ eventually approaches v_{nl} for the cubic Allen-Cahn equation. Therefore, we leave this as an outlook for further work. Due to the restriction of finite domain size in *auto07p* it was impossible for us to develop the whole bifurcation diagram for the quintic Allen-Cahn equation. Especially, we were unable to find the bifurcation of the solution branch corresponding to the front propagating from the stable state over the metastable state into the unstable state. We assume the front profiles obtained for $v_{nl} < v_l$ to be unstable. Therefore, we determined numerically the time evolution of fronts for $\mu = 0.05$ and for $\mu = 0.1$. We expect the fronts to be unstable for $\mu = 0.05$ whereas the profile at $\mu = 0.1$ needs to be stable (see figure 2.4(a)). We implemented a finite difference method and a four step Runge Kutta method. However, as we are not able to determine the homogenous states

of the system analytically we can only consider numerical data which we obtain with *auto07p*. In figure 4.1 we show four different front profiles at different times and μ values. The solutions at the top correspond to $\mu = 0.1$. We show the initial condition as grey dotted lines in order to show that the profiles are indeed stable at time $t = t_1$ and later $t = t_2$. The bottom two panels show a front at $\mu = 0.05$ which becomes unstable at $t = t_2$ as it no longer propagates into the unstable state ϕ_u^- but evolves into a front between the two stable states. However, at further time $t \gg t_2$ the front solution at $\mu = 0.1$ also becomes unstable. We ruled out boundary effects as a cause for this. A front propagating from $\phi_s^+ = 1$ into $\phi_u^+ = 0.5$ at $\mu = 0$ is stable at all times. When changing slightly the numerically obtained value for ϕ_u^- the front solution at $\mu = 0.1$ becomes unstable at earlier time $t \approx t_2$.

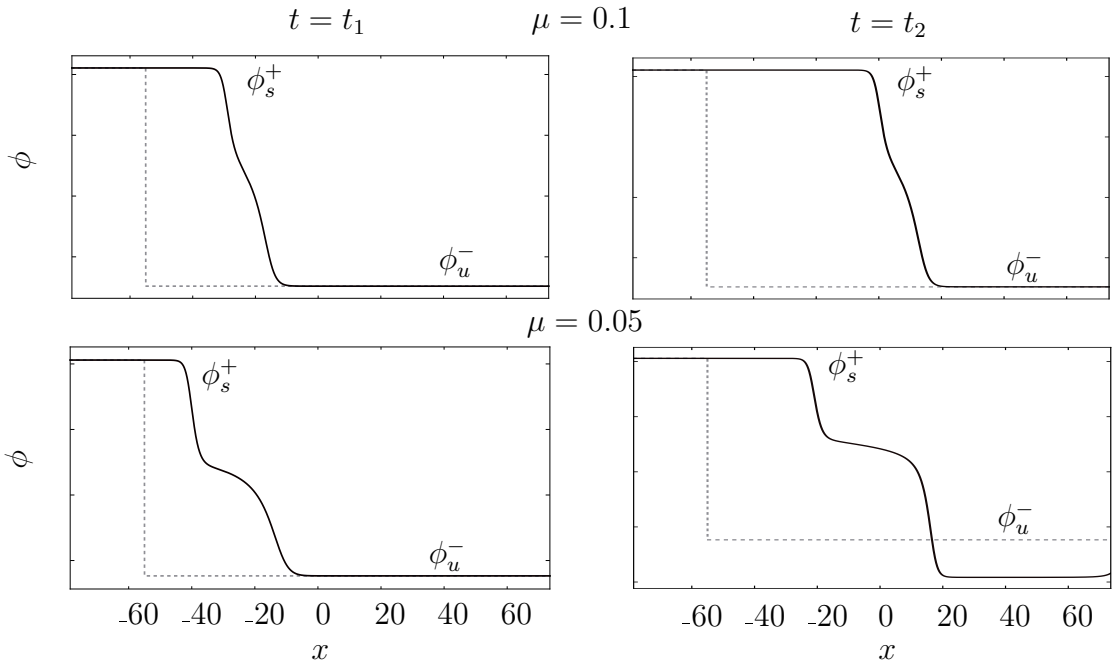

Figure 4.1: Time evolution of fronts propagating from ϕ_s^+ into ϕ_u^-. The corresponding solution branch is depicted in figure 2.4 as the blue dashed line. The grey dotted lines represent the initial condition.
Top: For $\mu = 0.1$ we expect the profiles to be stable and they are indeed at time $t = t_1$ and $t = t_2$.
Bottom: At $\mu = 0.05$ we assume the front to be unstable as $v_{nl} < v_l$. The bottom right panel shows, that the front indeed becomes unstable as it no longer propagates into the initial state ϕ_u^- at $t = t_2$.

Hence, we assume the inaccuracy of the numerically obtained data for the homogeneous solutions of the system to be one reason for a front profile at $\mu = 0.1$ to become unstable. However, we leave this and further examinations as an outlook as for example the determination of velocities at corresponding μ values. Moreover,

we need to overcome the finite size effects in the continuation. Additionally, we could study a quintic non-variational Allen-Cahn equation or examine the behavior of the bifurcation diagram for the cubic Allen-Cahn equation, when studying other non-variational terms. Finally, we could also examine on two dimensional fronts.

A. Appendix

A.1. Nonlinear marginal analysis for the cubic Allen-Cahn equation: Overdetermined equation system

In section 1.6 we obtain an overdetermined system of equation. Hence, we need to show, that the solution (1.73d) and (1.73e), i.e,

$$v = 3a_2(\phi^0 + \phi^s) \qquad \text{with} \qquad a_2 = \pm\frac{1}{\sqrt{2}}\,, \tag{A.1}$$

also satisfies (1.73b) and (1.73c):

$$-va_2b = a_2^2bc + \mu \tag{A.2a}$$
$$-va_2c = 2a_2^2b + a_2^2c^2 + 1\,. \tag{A.2b}$$

with

$$b = \phi^0\phi^s \tag{A.3a}$$
$$c = -\left(\phi^s + \phi^0\right) \tag{A.3b}$$

As we can not solve this analytically, we introduce $w_\pm^1(\mu)$ and $w_\pm^2(\mu)$. Therefore, we insert (A.1) and (A.3) into (A.2) and transform (A.2) such that the left hand sides are zero. We define the terms on the right-hand sides as:

$$w_\pm^1(\mu) = \mu + \left[\phi^0(\mu) + \phi^\pm(\mu)\right]\phi^0(\mu)\phi^\pm(\mu) \tag{A.4}$$
$$w_\pm^2(\mu) = 1 + \phi^0(\mu)\phi^\pm(\mu) - \left[\phi^0(\mu) + \phi^\pm(\mu)\right]^2\,, \tag{A.5}$$

which we require to be zero for all $-\mu_c < \mu < \mu_c$.

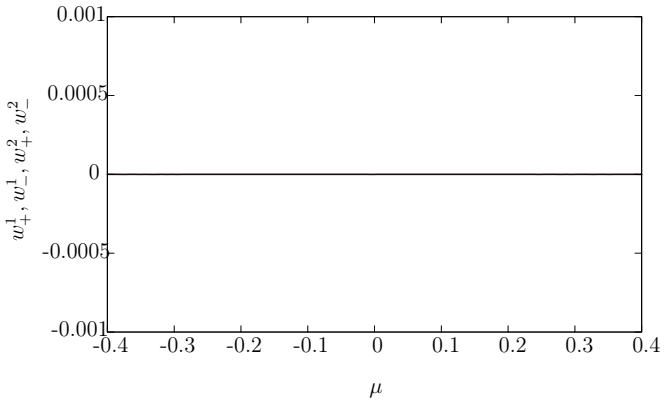

Figure A.1: The functions $w_\pm^1(\mu)$ and $w_\pm^2(\mu)$ are zero on the relevant μ interval.

We plotted $w_+^1(\mu)$ as illustrated in figure $A.1$ and find the expected result as well as for $w_\pm^2$ and w_-^1.

A.2. Nonlinear marginal analysis for the cubic Allen-Cahn equation: Calculation of crossing points

To calculate the point, where the linear and nonlinear marginal velocity, and the corresponding wave vectors are identical for section 1.6 we solve the system of equations:

$$v_{nl} = \frac{3}{\sqrt{2}}\left(\phi^0 + \phi^+\right) = 2\sqrt{1-3(\phi^0)^2} = v_l \tag{A.6}$$

$$k_{nl} = \frac{1}{\sqrt{2}}\left(-\phi^0 + \phi^+\right) = \sqrt{1-3(\phi^0)^2} = k_l \tag{A.7}$$

We multiply (A.7) by 2 and subtract it from (A.6) to obtain

$$\frac{5}{\sqrt{2}}\phi^0 + \frac{1}{\sqrt{2}}\phi^+ = 0 \tag{A.8}$$

We solve this by rewriting ϕ^0 and ϕ^+:

$$\phi^0 = -\sqrt{\frac{4}{3}}\cos\left(\frac{1}{3}\arccos\left(\frac{3\sqrt{3}}{2}\mu\right) + \frac{\pi}{3}\right) := -A\cos\left(\alpha(\mu) + \beta\right) \tag{A.9a}$$

$$\phi^+ = \sqrt{\frac{4}{3}}\cos\left(\frac{1}{3}\arccos\left(\frac{3\sqrt{3}}{2}\mu\right)\right) := A\cos\left(\alpha(\mu)\right) \tag{A.9b}$$

with :

$$\alpha(\mu) = \frac{1}{3}\arccos\left(\frac{3\sqrt{3}}{2}\mu\right) \tag{A.9c}$$

$$\beta = \frac{\pi}{3} \tag{A.9d}$$

Inserting (A.9a) and (A.9b) into (A.8) yields:

$$5\cos\left(\alpha(\mu) + \beta\right) = \cos\left(\alpha(\mu)\right)\ . \tag{A.10}$$

Applying the trigonometric identity

$$\cos\left(\alpha(\mu) \pm \beta\right) = \cos(\alpha)\cos(\beta) \mp \sin(\alpha)\sin(\beta) \tag{A.11}$$

and divide by $\cos(\alpha)$ which is unequal to zero, as $\phi^+ > 0$ in the valid interval for μ, we obtain:

$$5\cos(\beta) - 5\tan(\alpha)\sin(\beta) = 1 \tag{A.12}$$

$$\Leftrightarrow \alpha = \arctan\left(\frac{5\cos(\beta) - 1}{5\sin\beta}\right) \tag{A.13}$$

Employing (A.9c) and (A.9d) this finally leads to:

$$\Rightarrow \mu = \frac{2}{3\sqrt{3}}\cos\left(3\arctan\left(\frac{\frac{5}{2} - 1}{\frac{5\sqrt{3}}{2}}\right)\right) \approx 0.2078\,. \tag{A.14}$$

Analogously, we can calculate the point in figure 1.7 where the red dashed and the green dotted branches cross each other. We first need to show that

$$\phi^+ + \phi^- + \phi^0 = 0\,. \tag{A.15}$$

Therefore, we employ (A.9a) and (A.9b) and also introduce:

$$\phi^- = -\sqrt{\frac{4}{3}}\cos\left(\frac{1}{3}\arccos\left(\frac{3\sqrt{3}}{2}\mu\right) - \frac{\pi}{3}\right) = -A\cos\left(\alpha(\mu) - \beta\right)\,. \tag{A.16}$$

Inserting (A.9a), (A.9b) and (A.16) into (A.15)

$$A\cos\left(\alpha(\mu)\right) - A\cos\left(\alpha(\mu) - \beta\right) - A\cos\left(\alpha(\mu) + \beta\right) = 0\,, \tag{A.17}$$

and again using the trigonometric identity (A.11) leads to

$$A\cos\left(\alpha\right) - A\cos(\alpha)\cos(\beta) + A\sin(\alpha)\sin(\beta) - A\cos(\alpha)\cos(\beta) - A\sin(\alpha)\sin(\beta) = 0\,. \tag{A.18}$$

With (A.9d) we obtain the requested identity

$$-A\cos\left(\alpha\right)\left[2\cos(\beta) - 1\right] = 0 \tag{A.19}$$

$$0 = 0\,. \tag{A.20}$$

Now, we can determine the crossing point with

$$v_l = 2\sqrt{1 - 3(\phi^0)^2} = \frac{3}{\sqrt{2}}\left(\phi^- + \phi^+\right) = v_s\,. \tag{A.21}$$

With (A.15) we can insert

$$\phi^+ + \phi^- = -\phi^0 \tag{A.22}$$

on the right-hand side of (A.21) and square the whole equation

$$4(1-3(\phi^0)^2) = \frac{9}{2}\left(\phi^0\right)^2 \tag{A.23}$$

which finally yields:

$$\phi^0 = 2\sqrt{2}\,, \tag{A.24}$$

where we only focus on the positive root. Employing now the expressions for α (A.9c) and β (A.9d) we obtain as crossing point

$$\mu = \frac{2}{3\sqrt{3}}\cos\left(3\left(\cos^{-1}\left(\sqrt{\frac{2}{11}}\right) - \frac{\pi}{3}\right)\right) \approx 0.3730\,. \tag{A.25}$$

A.3. Nonlinear marginal analysis for the cubic Allen-Cahn equation: Front solution

We need to integrate

$$h(\phi) = a_0 + a_1\phi + a_2\phi^2 = \frac{\mathrm{d}\phi}{\mathrm{d}\xi} \tag{A.26}$$

in order to get the front profile $\phi(\xi)$. Thus, we obtain:

$$\begin{aligned}
\xi + q &= \int \frac{1}{h(\phi)}\mathrm{d}\phi \qquad q = \text{const.} \\
&= \int \left(a_0 + a_1\phi + a_2\phi^2\right)^{-1} \mathrm{d}\phi \\
&= \int \frac{1}{a_2}\left(\phi^2 + \frac{a_1}{a_2}\phi + \frac{a_0}{a_2}\right)^{-1} \mathrm{d}\phi \\
&= \int \frac{1}{a_2}\left(\left(\phi + \frac{a_1}{2a_2}\right)^2 - \frac{a_1^2}{4a_2^2} + \frac{a_0}{a_2}\right)^{-1} \mathrm{d}\phi \\
\text{substitution} : u &= \phi + \frac{a_1}{2a_2} \qquad \frac{\mathrm{d}u}{\mathrm{d}\phi} = 1 \\
&= \int \frac{1}{a_2}\left(u^2 - \frac{a_1^2}{4a_2^2} + \frac{a_0}{a_2}\right)^{-1} \mathrm{d}u \\
&= \frac{1}{a_2}\left(\frac{a_1^2}{4a_2^2} - \frac{a_0}{a_2}\right)^{-1} \int \left(u^2 \left(\frac{a_1^2}{4a_2^2} - \frac{a_0}{a_2}\right)^{-1} - 1\right)^{-1} \mathrm{d}u \\
\text{substitution} : w &= u\left(\frac{a_1^2}{4a_2^2} - \frac{a_0}{a_2}\right)^{-\frac{1}{2}} \qquad \frac{\mathrm{d}w}{\mathrm{d}u} = \left(\frac{a_1^2}{4a_2^2} - \frac{a_0}{a_2}\right)^{-\frac{1}{2}} \\
&= -\frac{1}{a_2}\left(\frac{a_1^2}{4a_2^2} - \frac{a_0}{a_2}\right)^{-\frac{1}{2}} \int \left(1 - w^2\right) \mathrm{d}w \\
\xi + \tilde{q} &= -\frac{1}{a_2}\left(\frac{a_1^2}{4a_2^2} - \frac{a_0}{a_2}\right)^{-\frac{1}{2}} \operatorname{arctanh}(w) \qquad \tilde{q} = \text{const.}
\end{aligned}$$

back substitution

$$= -\frac{1}{a_2}\left(\frac{a_1^2}{4a_2^2} - \frac{a_0}{a_2}\right)^{-\frac{1}{2}} \operatorname{arctanh}\left(\left(\phi + \frac{a_1}{2a_2}\right)\left(\frac{a_1^2}{4a_2^2} - \frac{a_0}{a_2}\right)^{-\frac{1}{2}}\right) \tag{A.28}$$

we can now solve this for $\phi(\xi)$:

$$\phi(\xi) = \left(\frac{a_1^2}{4a_2^2} - \frac{a_0}{a_2}\right)^{\frac{1}{2}} \tanh\left(-a_2\left(\frac{a_1^2}{4a_2^2} - \frac{a_0}{a_2}\right)^{\frac{1}{2}}(\xi + \tilde{q})\right) - \frac{a_1}{2a_2} \tag{A.29}$$

$$a_0 = \frac{1}{\sqrt{2}}\phi^0\phi^s \tag{A.30}$$

$$a_1 = -\frac{1}{\sqrt{2}}\left(\phi^s + \phi^0\right) \tag{A.31}$$

$$a_2 = \frac{1}{\sqrt{2}} \tag{A.32}$$

$$\Rightarrow \phi(\xi) = \frac{1}{2}|\phi^0 - \phi^s|\tanh\left(-\frac{1}{2\sqrt{2}}|\phi^0 - \phi^s|\xi\right) + \frac{1}{2}(\phi^0 + \phi^s)\,, \tag{A.33}$$

where we set $\tilde{q} = 0$ due to boundary conditions ($\phi(\xi \to \infty) = 1$, $\phi(\xi \to -\infty) = -1$ at $\mu = 0$).

A.4. Velocity determination for variational cubic Allen-Cahn equation

In section 3 we examine

$$\frac{\partial\phi}{\partial t} = \frac{\partial^2\phi}{\partial x^2} + \phi - \phi^3 + \mu + \epsilon\left(\frac{\partial\phi}{\partial x}\right)^2 + 2\phi\frac{\partial^2\phi}{\partial x^2}\,, \tag{A.34}$$

with $b = 1$. Hence, (A.34) is variational and we can determine the velocity, analogously to section 1.1 by transforming to the comoving frame $\xi = x - v_0 t$

$$-v_0\frac{\mathrm{d}\phi}{\mathrm{d}\xi} = \frac{\mathrm{d}^2\phi}{\mathrm{d}\xi^2} + \phi - \phi^3 + \mu + \epsilon\left(\frac{\mathrm{d}\phi}{\mathrm{d}\xi}\right)^2 + 2b\phi\frac{\mathrm{d}^2\phi}{\mathrm{d}\xi^2}\,. \tag{A.35}$$

Multiplying (A.35) by $\mathrm{d}_\xi\phi$

$$-v_0\left(\frac{\mathrm{d}\phi}{\mathrm{d}\xi}\right)^2 = \frac{1}{2}\frac{\mathrm{d}}{\mathrm{d}\xi}\left(\frac{\mathrm{d}\phi}{\mathrm{d}\xi}\right)^2 - \frac{\mathrm{d}}{\mathrm{d}\xi}f(\phi) + \epsilon\frac{\mathrm{d}}{\mathrm{d}\xi}\left(\phi\left(\frac{\mathrm{d}\phi}{\mathrm{d}\xi}\right)^2\right)\,, \tag{A.36}$$

where we employed that

$$\frac{\mathrm{d}}{\mathrm{d}\xi}\left(\phi\left(\frac{\mathrm{d}\phi}{\mathrm{d}\xi}\right)^2\right) = \frac{\mathrm{d}\phi}{\mathrm{d}\xi}\left(\frac{\mathrm{d}\phi}{\mathrm{d}\xi}\right)^2 + 2\phi\frac{\mathrm{d}\phi}{\mathrm{d}\xi}\frac{\mathrm{d}^2\phi}{\mathrm{d}\xi^2} = \frac{\mathrm{d}\phi}{\mathrm{d}\xi}g_{nv}\,. \tag{A.37}$$

Thus, integrating (A.35) yields

$$-v_0 \int_{-\infty}^{\infty} \left(\frac{\mathrm{d}\phi}{\mathrm{d}\xi}\right)^2 \mathrm{d}\xi = \frac{1}{2}\int_{-\infty}^{\infty} \frac{\mathrm{d}}{\mathrm{d}\xi}\left(\frac{\mathrm{d}\phi}{\mathrm{d}\xi}\right)^2 \mathrm{d}\xi - \int_{-\infty}^{\infty} \frac{\mathrm{d}}{\mathrm{d}\xi} f(\phi)\,\mathrm{d}\xi + \epsilon \int_{-\infty}^{\infty} \frac{\mathrm{d}}{\mathrm{d}\xi}\left(\phi\left(\frac{\mathrm{d}\phi}{\mathrm{d}\xi}\right)^2\right) \mathrm{d}\xi\,. \quad \text{(A.38)}$$

Applying Neumann boundary condition implies, that first and third term on the right-hand side become zero. Hence, we finally obtain

$$v_0 = \pm \frac{f\left(\phi^i\right) - f\left(\phi^f\right)}{\int_{-\infty}^{\infty}\left(\frac{\mathrm{d}\phi}{\mathrm{d}\xi}\right)^2 \mathrm{d}\xi}\,. \quad \text{(A.39)}$$

This is identical to the velocity determined in section 1.1.

A.5. Velocity determination for non-variational cubic Allen-Cahn equation at $\mu = 0$

In order to determine the velocity of a front propagating from ϕ^+ into ϕ^- at $\mu = 0$ for section 3 we consider

$$v_1 = \frac{\int_{-\infty}^{\infty}\left(\left(\frac{\partial\phi}{\partial x}\right)^2 + 2b\phi\frac{\partial^2\phi}{\partial x^2}\left(\phi_F(\xi)\right)\right)\partial_\xi\phi_F\,\mathrm{d}\xi}{\int_{-\infty}^{\infty}\left(\partial_\xi\phi_F\right)^2\,\mathrm{d}\xi}\,, \quad \text{(A.40)}$$

with

$$\phi_F(\xi) = \tanh\left(-\frac{1}{\sqrt{2}}\xi\right)\,. \quad \text{(A.41)}$$

Note, that we employed partial derivative for the determination of the velocity shift, as our initial ϕ depends on ζ and t. However, we can now change to total derivatives as ϕ_F only depends on ξ. Firstly, we examine the numerator in (A.40)

$$\int_{-\infty}^{\infty}\left(\frac{\mathrm{d}\phi_F}{\mathrm{d}\xi}\right)^2\frac{\mathrm{d}\phi_F}{\mathrm{d}\xi} + 2b\phi_F\frac{\mathrm{d}^2\phi_F}{\mathrm{d}\xi^2}\frac{\mathrm{d}\phi_F}{\mathrm{d}\xi}\,\mathrm{d}\xi\,. \quad \text{(A.42)}$$

We can rewrite the first term in the integral employing partial integration and Neumann boundary condition

$$\int_{-\infty}^{\infty}\left(\frac{\mathrm{d}\phi_F}{\mathrm{d}\xi}\right)^2\frac{\mathrm{d}\phi_F}{\mathrm{d}\xi}\,\mathrm{d}\xi = \left[\phi_F\frac{\mathrm{d}^2\phi_F}{\mathrm{d}\xi^2}\right]_{-\infty}^{\infty} - 2\int_{-\infty}^{\infty}\phi_F\frac{\mathrm{d}^2\phi_F}{\mathrm{d}\xi^2}\frac{\mathrm{d}\phi_F}{\mathrm{d}\xi}\,\mathrm{d}\xi \quad \text{(A.43a)}$$

$$= -2\int_{-\infty}^{\infty}\phi_F\frac{\mathrm{d}^2\phi_F}{\mathrm{d}\xi^2}\frac{\mathrm{d}\phi_F}{\mathrm{d}\xi}\,\mathrm{d}\xi\,. \quad \text{(A.43b)}$$

Thus (A.42) becomes

$$\int_{-\infty}^{\infty} 2(b-1)\phi_F \frac{\mathrm{d}^2\phi_F}{\mathrm{d}\xi^2}\frac{\mathrm{d}\phi_F}{\mathrm{d}\xi}\,\mathrm{d}\xi\,. \tag{A.44}$$

Inserting (A.41) into (A.44) and using $\partial_x \tan(x) = 1 - \tan^2(x)$, we obtain for the numerator

$$\int_{-\infty}^{\infty} \sqrt{2}(b-1)\left[\tanh^2\left(-\frac{1}{\sqrt{2}}\xi\right)\left(1-\tanh^2\left(-\frac{1}{\sqrt{2}}\xi\right)\right)^2\right]\mathrm{d}\xi\,. \tag{A.45}$$

Employing the substitution

$$u(\xi) = \tanh\left(-\frac{1}{\sqrt{2}}\xi\right) \tag{A.46a}$$

$$\frac{\mathrm{d}u}{\mathrm{d}\xi} = -\frac{1}{\sqrt{2}}\left(1-\tanh^2\left(-\frac{1}{\sqrt{2}}\xi\right)\right)\,, \tag{A.46b}$$

(A.44) transforms to

$$-\int_1^{-1} 2(b-1)\left[u^2\left(1-u^2\right)\right]\mathrm{d}u = -2(b-1)\left[\frac{1}{3}u^3 - \frac{1}{5}u^5\right]_1^{-1} = (b-1)\frac{8}{15}\,. \tag{A.47}$$

Inserting (A.41) into the denominator

$$\int_{-\infty}^{\infty}\left(\partial_\xi\phi_F\right)^2\,\mathrm{d}\xi = \frac{1}{2}\int_{-\infty}^{\infty}\left[1-\tanh^2\left(-\frac{1}{\sqrt{2}}\xi\right)\right]\mathrm{d}\xi\,, \tag{A.48}$$

and again using the substitution (A.46) yields for (A.48)

$$-\int_1^{-1}\frac{1}{\sqrt{2}}\left(1-u^2\right)\,\mathrm{d}u = -\frac{1}{\sqrt{2}}\left[u-\frac{1}{3}u^3\right]_1^{-1} = \frac{4}{3\sqrt{2}}\,. \tag{A.49}$$

Thus dividing (A.47) by (A.49) we finally obtain the velocity for $b = 2$

$$v_1 = (b-1)\frac{2\sqrt{2}}{5} = \frac{2\sqrt{2}}{5}\,. \tag{A.50}$$

B. References

[1] J.S. Langer. *Solids Far from Equilibrium* -. Cambridge University Press, Cambridge, 1991.

[2] Guenter Ahlers and David S. Cannell. Vortex-front propagation in rotating couette-taylor flow. *Phys. Rev. Lett.*, 50:1583–1586, May 1983.

[3] Jay Fineberg and Victor Steinberg. Vortex-front propagation in rayleigh-bénard convection. *Phys. Rev. Lett.*, 58:1332–1335, Mar 1987.

[4] J. S. Langer. Instabilities and pattern formation in crystal growth. *Rev. Mod. Phys.*, 52:1–28, Jan 1980.

[5] Maria Burger. *Oscillations and Traveling Waves in Chemical Systems* -. Wiley, New York, 1985.

[6] John Bechhoefer, Hartmut Löwen, and Laurette S. Tuckerman. Dynamical mechanism for the formation of metastable phases. *Phys. Rev. Lett.*, 67:1266–1269, Sep 1991.

[7] Wim van Saarloos. Front propagation into unstable states. ii. linear versus nonlinear marginal stability and rate of convergence. *Phys. Rev. A*, 39:6367–6390, Jun 1989.

[8] Arnaud Couairon and Jean-Marc Chomaz. Absolute and convective instabilities, front velocities and global modes in nonlinear systems. *Physica D: Nonlinear Phenomena*, 108(3):236 – 276, 1997.

[9] James A. Powell, Alan C. Newell, and Christopher K. R. T. Jones. Competition between generic and nongeneric fronts in envelope equations. *Phys. Rev. A*, 44:3636–3652, Sep 1991.

[10] G. Kozyreff and M. Tlidi. Nonvariational real Swift-Hohenberg equation for biological, chemical, and optical systems. *Chaos*, 17(3):037103, September 2007.

[11] A. J. Alvarez-Socorro, M. G. Clerc, G. González-Cortés, and M. Wilson. Nonvariational mechanism of front propagation: Theory and experiments. *Phys. Rev. E*, 95:010202, Jan 2017.

[12] L.M. Pismen. *Patterns and Interfaces in Dissipative Dynamics* -. Springer Science Business Media, Berlin Heidelberg, 2006.

[13] E. Ben-Jacob, H. Brand, G. Dee, L. Kramer, and J.S. Langer. Pattern propagation in nonlinear dissipative systems. *Physica D: Nonlinear Phenomena*, 14(3):348 – 364, 1985.

[14] Ute Ebert and Wim van Saarloos. Front propagation into unstable states: universal algebraic convergence towards uniformly translating pulled fronts. *Physica D: Nonlinear Phenomena*, 146(1):1 – 99, 2000.

[15] D.G Aronson and H.F Weinberger. Multidimensional nonlinear diffusion arising in population genetics. *Advances in Mathematics*, 30(1):33 – 76, 1978.

[16] G. C. Paquette, Lin-Yuan Chen, Nigel Goldenfeld, and Y. Oono. Structural stability and renormalization group for propagating fronts. *Phys. Rev. Lett.*, 72:76–79, Jan 1994.

[17] Wim van Saarloos. Front propagation into unstable states: Marginal stability as a dynamical mechanism for velocity selection. *Phys. Rev. A*, 37:211–229, Jan 1988.

[18] R. D. Benguria and M. C. Depassier. Speed of fronts of the reaction-diffusion equation. *Phys. Rev. Lett.*, 77:1171–1173, Aug 1996.

[19] Rüdiger U. Seydel. *Practical Bifurcation and Stability Analysis* -. Springer Science Business Media, Berlin Heidelberg, 2009.

[20] Eusebius J. Doedel, Thomas F. Fairgrieve, Björn Sandstede, Alan R. Champneys, Yuri A. Kuznetsov, and Xianjun Wang. Auto-07p: Continuation and bifurcation software for ordinary differential equations. Technical report, 2007.

[21] A. G. Ramm. A simple proof of the fredholm alternative and a characterization of the fredholm operators. *The American Mathematical Monthly*, 108(9):855–860, 2001.

Acknowledgement

At this point I would like to thank my supervisors Uwe Thiele and Svetlana Gurevich for providing me an interesting topic and challenging and supporting me during the work for this thesis.
I would also like to thank Walter Tewes for all the valuable advices.
Furthermore, I thank the people in the working group, especially those working in the same office for good advices and nice coffee breaks.
Special thanks go to Tobias Frohoff-Hülsmann who never hesitated to discuss my results with me and always offered good advice and support.
I thank my family who were always there for either support or distraction from my studies.
Finally, I thank my friends for all the good (physics related and not physics related) times we spent together.

Declaration of Academic Integrity

I hereby confirm that this thesis on 'Front motion in Allen-Cahn-type equations' is solely my own work and that I have used no sources or aids other than the ones stated. All passages in my thesis for which other sources, including electronic media, have been used, be it direct quotes or content references, have been acknowledged as such and the sources cited.

_____

(date and signature of student)

I agree to have my thesis checked in order to rule out potential similarities with other works and to have my thesis stored in a database for this purpose.

_____

(date and signature of student)